



Universidade Federal do Piauí
Centro de Ciências da Natureza
Departamento de Física
Programa de Pós-Graduação em Física

Maria Lúcia Álvares Paz

Electronic Properties of Two-dimensional and One-dimensional Carbon Allotropes with Non-hexagonal Rings

**Propriedades Eletrônicas de Alótropos de Carbono
Unidimensionais e Bidimensionais com Anéis
Não-hexagonais**

Teresina - PI

2019

Maria Lúcia Álvares Paz

**Electronic Properties of Two-dimensional and
One-dimensional Carbon Allotropes with Non-hexagonal
Rings**

**Propriedades Eletrônicas de Alótropos de Carbono
Unidimensionais e Bidimensionais com Anéis
Não-hexagonais**

Dissertação de Mestrado apresentada ao Programa de Pós-Graduação em Física da Universidade Federal do Piauí como requisito parcial para a obtenção do Título de Mestre em Física.

Teresina - PI

2019

FICHA CATALOGRÁFICA

Serviço de Processamento Técnico da Universidade Federal do Piauí
Biblioteca Setorial de Ciências da Natureza - CCN

P348p Paz, Maria Lúcia Álvares.
Propriedades eletrônicas de alótropos de carbono unidimensionais e bidimensionais com âneos não-hexagonais / Maria Lúcia Álvares Paz. – Teresina: 2019.
74 f. il. color

Dissertação (Mestrado) – Universidade Federal do Piauí, Centro de Ciências da Natureza, Pós-graduação em Física, 2019.

Orientador: Prof. Dr. Eduardo Costa Girão.

1. Matéria Condensada. 2. Propriedades eletrônicas. 3. Naftileno. I. Título.

CDD 530.41

Bibliotecária: Caryne Maria da Silva Gomes CRB3-1461

“Propriedades Eletrônicas de Alótropos de Carbono Unidimensionais e Bidimensionais com Anéis Não-hexagonais - Electronic Properties of Two-dimensional and One-dimensional Carbon Allotropes with Non-Hexagonal Rings “

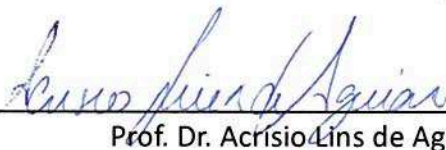
Maria Lúcia Álvares Paz

Dissertação de Mestrado apresentada ao Programa de Pós-Graduação em Física do Centro de Ciências da Natureza - CCN/UFPI.

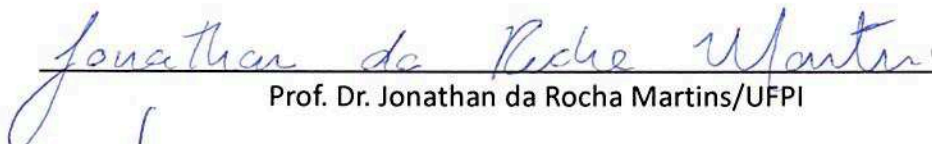
Comissão Julgadora:



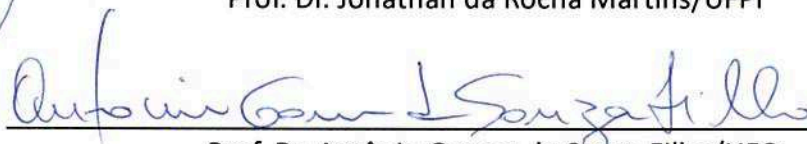
Prof. Dr. Eduardo Costa Girão(Orientador)



Prof. Dr. Acrísio Lins de Aguiar/UFPI



Prof. Dr. Jonathan da Rocha Martins/UFPI



Prof. Dr. Antônio Gomes de Souza Filho/UFC

Aprovada em 31/01/2019

Acknowledgements

First of all, I thank God for my life and for everything he has helped me to achieve, always showing me what really matters in life.

I thank my family, for always supporting my decisions, understanding my constant absence, and believing that my dreams are worthy.

I also want to thank all the teachers who contributed to my training and to my life in general. Many with lessons that go beyond the classroom.

I thank my friends for all the deep conversations, and the moments we have spent together. All these moments have matured us a lot, and some days it would be impossible to get through them without the support and love they give me.

Finally, I would like to thank my advisor Eduardo Costa Girão, for entrusting me with this work and believing that I could accomplish it. Thanks for your patience and encouragement. Also, I want to thank my co-advisor Aldilene Saraiva for all the help, discussions and also for the motivation she has given me during this time.

“Beyond mountains, more mountains.”

Haitian Proverb

Abstract

Carbon is one of the most abundant elements in nature. The different hybridizations allowed for carbon enable it to form distinct materials with a variety of dimensions, which is a feature strongly related to the electronic properties of the carbon materials. Since the properties of these carbon-based materials are directly related to their atomic structures, it is needed a deep understanding of the relationship between these two features. Therefore, such electronic features has motivated the investigation of many two-dimensional materials (beyond graphene, which is a zero gap semiconductor), such as graphenylene, phagraphene, haecklites, and others. Therefore, considering the idea of sp^2 carbon systems with a structural unit different from that of graphene, such as graphenylene, we propose in this work a hypothetical 2D-system where the structural unit is a naphthyl group. According to the way these naphthyl units are arranged in the structure, we can build two different 2D-networks. We named the first one as naphthylene- α , and the second one as naphthylene- β . Besides performing calculations on these two-dimensional systems, we also proposed and investigated the electronic properties of different families of nanoribbons that can be constructed from these 2D-systems. All calculations were performed using Density Functional Theory as implemented in the SIESTA code. Our study shows that most of the investigated systems present a metallic behavior, and the states close to the Fermi level are not edge states as in graphene nanoribbons, but rather they are distributed over the internal regions of the structures.

Key-words: Electronic structure, density functional theory, naphthylene, non-hexagonal rings.

Resumo

O carbono é um dos elementos mais abundantes na natureza. As diferentes hibridizações possíveis para o carbono permitem que ele forme materiais distintos com uma variedade de dimensões, o que é uma característica fortemente relacionada às propriedades eletrônicas do átomo de carbono. Como as propriedades desses materiais à base de carbono estão diretamente relacionadas às suas estruturas atômicas, é necessário um profundo entendimento da relação entre essas duas características. Portanto, isso tem motivado a investigação de muitos materiais bidimensionais (além do grafeno, que é um semicondutor de gap zero), tais como graphenylene, phagraphene, haecklites, etc. Logo, considerando a idéia de sistemas de carbono com hibridização sp^2 e com uma unidade estrutural diferente da do grafeno, como o graphenylene por exemplo, propomos neste trabalho investigar um sistema bidimensional onde a unidade estrutural é um grupo naftil. De acordo com o modo como estas unidades de naftil estão dispostas na estrutura, podemos ter duas redes 2D diferentes. Nomeamos o primeiro sistema como naphthylene- α , e o segundo como naphthylene- β . Além de estudarmos esses sistemas bidimensionais, também investigamos as propriedades eletrônicas de diferentes famílias de nanofitas que podem ser construídas a partir desses sistemas 2D. Todos os cálculos foram realizados utilizando a Teoria do Funcional da Densidade por meio do código SIESTA. Nossos estudos mostram que a maioria dos sistemas investigados apresenta um comportamento metálico, e os estados próximos ao nível de Fermi não são estados de borda como nas nanofitas de grafeno, mas são distribuídos ao longo de toda a estrutura.

Palavras-chave: Estrutura eletrônica, teoria do funcional da densidade, naftileno, anéis não-hexagonais.

List of Figures

1.1	Schematic representation of a) graphene, b) graphite, c) carbon nanotube, and d) fullerene, which are different allotropes of carbon.	15
1.2	Direct lattice of graphene.	16
1.3	Reciprocal lattice of graphene and its 1st Brillouin zone highlighted as gray. . .	17
1.4	a) Electronic band structure over the whole BZ (adapted from [18]) and b) along the high symmetry direction in the first Brillouin zone.	19
1.5	Schematic representation of bottom-up and top-down approaches. Adapted from [27].	20
1.6	(a) Transmission electron microscopy (TEM) image of carbon nanoparticles, (b) carbon nanoribbons and (c) graphene sheets produced by electrochemical exfoliation [29, 30].	20
1.7	a) Scanning electron microscopy (SEM) images of grown graphene films on thin (300-nm) nickel layers and thick (1-mm) Ni foils (inset). b) TEM images of graphene films of different thicknesses [32].	21
1.8	Directions of high symmetry in graphene.	23
1.9	Atomic structure of a) zigzag and b) armchair graphene nanoribbons. The boxes in red highlight the unit cell of each nanoribbon.	23
1.10	Atomic structure of a) zigzag graphene nanoribbon and b) armchair graphene nanoribbon along with their electronic band structures. The boxes in red highlight the unit cell.	24
1.11	Electronic band structure of zigzag graphene nanoribbon a) with AFM orientation and b) FM orientation.	25
1.12	Variation of the band gaps os AGNRs as a function of the ribbon width (W_a). Adapted from [42].	25
1.13	Atomic structure of biphenylene, amorphous graphene and phagraphene. Adapted from [43].	26

1.14	a) Atomic structure of graphenylene along with b) its electronic band structure [24].	27
1.15	c) electronic band structure of graphenylene nanoribbon with zigzag edge and d) armchair edge, respectively. Adapted from [24].	27
1.16	Basic building block of a) graphenylene and b) naphthylene- α and naphthylene- β systems, c) naphthylene- α sheet, d) naphthylene- β sheet.	28
2.1	Representation of the self-consistent loop for solution of Kohn-Sham equation [62].	37
3.1	a) Naphthylene- α atomic structure together with its unit cell, b) Electronic band structure of naphthylene- α plotted along high-symmetry direction on the BZ, c) Plot of the valence and conduction bands over the entire BZ. The same information for naphthylene- β is displayed in d), e) and f), respectively.	44
3.2	C-C bond lengths (in Å) in naphthylene- α and naphthylene- β , respectively. . .	44
3.3	a) α ZNNR-hsh ($w = 1$), b) α ZNNR-hsh ($w = 2$), c) α ZNNR-hsh ($w = 3$), d) α ZNNR-hh ($w = 1$), e) α ZNNR-hh ($w = 2$), f) α ZNNR-hh ($w = 3$) nanoribbons. The box in red highlights the unit cell of the nanoribbons.	46
3.4	a) α ANNR-h ($w = 1$), b) α ANNR-h ($w = 2$), c) α ANNR-h ($w = 3$), d) α ANNR-hh ($w = 1$), e) α ANNR-hh ($w = 2$), f) α ANNR-hh ($w = 3$) nanoribbons. The box in red highlights the unit cell of the nanoribbons.	47
3.5	LDOS plot (front and side view) for α ZNNR-hsh a) $w = 1$, b) $w = 2$ and c) $w = 3$ nanoribbons from -0.1 eV to 0.1 eV around the Fermi level along with their electronic band structures. Isosurface value of 0.002.	49
3.6	LDOS plot (front and side view) for α ZNNR-hh a) $w = 1$, b) $w = 2$, and c) $w = 3$ nanoribbons from -0.1 eV to 0.1 eV around the Fermi level along with their electronic band structures. Isosurface value of 0.002.	50
3.7	LDOS plot (front and side view) for α ANNR-h a) $w = 1$, b) $w = 2$, and c) $w = 3$ nanoribbons from -0.1 eV to 0.1 eV (except for ($w = 2$)) around the Fermi level along with their electronic band structures. Isosurface value of 0.002.	51
3.8	LDOS plot (front and side view) for α ANNR-hh a) ($w = 1$), b) ($w = 2$), and c) ($w = 3$) nanoribbons from -0.1 eV to 0.1 eV around the Fermi level along with their electronic band structures. Isosurface value of 0.002.	52
3.9	a) α ANNR-h ($w = 1$), b) α ANNR-hh ($w = 1$) nanoribbons along with the electronic band structures for the non polarized (NP), antiferromagnetic (AFM) and ferromagnetic (FM) states, respectively.	54
3.10	Spin density distribution for the α ANNR-h ($w = 1$) structure.	55

3.11	Electronic band structure for spin up states, total DOS (spin up contribution) along with the PDOS (spin up contribution) from REGION 1 and REGION 2, LDOS plot for I and II bands (spin up contribution) around the Fermi level. Isosurface value of 0.0009 for LDOS plot.	55
3.12	a) Electronic band structure for spin down states, total DOS (spin down contribution) along with the PDOS (spin down contribution) from REGION 1 and REGION 2 and LDOS plot for the two bands (I) (spin down contribution) above the Fermi level. Isosurface value of 0.002 for LDOS plot.	56
3.13	a) β ANNR-hh ($w = 1$), b) β ANNR-hh ($w = 2$), c) β ANNR-hh ($w = 3$) nanoribbons. The box in red highlights the unit cell.	57
3.14	a) β ANNR-h ($w = 1$), b) β ANNR-h ($w = 1$), c) β ANNR-h ($w = 3$), d) β ZNNR-hh ($w = 1$), e) β ZNNR-hh ($w = 2$), f) β ZNNR-hh ($w = 3$) nanoribbons. The box in red highlights the unit cell.	58
3.15	LDOS plot (front and side view) for β ANNR-h a) ($w = 1$), b) ($w = 2$), and c) ($w = 3$) nanoribbons from -0.1 eV to 0.1 eV around the Fermi level along with their electronic band structures. Isosurface value of 0.006.	59
3.16	LDOS plot (front and side view) for β ANNR-hh a) ($w = 1$), b) ($w = 2$), and c) ($w = 3$) nanoribbons from -0.1 eV to 0.1 eV around the Fermi level along with their electronic band structures. Isosurface value of 0.0008.	60
3.17	LDOS plot (front and side view) for β ZNNR-hh a) ($w = 1$), b) ($w = 2$), and c) ($w = 3$) nanoribbons from -0.1 eV to 0.1 eV around the Fermi level along with their electronic band structures. Isosurface value of 0.0008.	61
3.18	a) β ANNR-hh ($w = 1$), b) β ANNR-hh ($w = 2$), and c) β ANNR-hh ($w = 3$) nanoribbons along with the electronic band structures for the non polarized (NP) and anti-ferromagnetic (AFM) states, respectively.	62
3.19	a) β ZNNR-hh ($w = 1$), b) β ZNNR-hh ($w = 2$) and c) β ZNNR-hh ($w = 3$) nanoribbons along with the electronic band structures for the paramagnetic (PM), antiferromagnetic (AFM) and ferromagnetic (FM) states, respectively.	63
3.20	Spin density distribution of a) β ANNR-hh ($w = 1$), b) β ANNR-hh ($w = 2$) and c) β ANNR-hh ($w = 3$) nanoribbons in the AFM state.	64
3.21	Spin density distribution of a) β ZNNR-hh ($w = 1$), b) β ZNNR-hh ($w = 2$) and c) β ZNNR-hh ($w = 3$) nanoribbons in the AFM and FM state.	65

List of Tables

- 3.1 Number of carbon atoms by unit cell as a function of the width of the ribbon. . 48
- 3.2 Number of carbon atoms by unit cell as a function of the width of the ribbon. . 59

Contents

1	Literature Review	14
1.1	Carbon Based Materials	14
1.2	Graphene	16
1.2.1	Structural Properties	16
1.2.2	Electronic Properties	18
1.2.3	Graphene Synthesis	19
1.2.4	Potentialities for Graphene-based Materials	21
1.3	Graphene Nanoribbons	22
1.4	Two-dimensional Carbon Networks	26
1.5	This Work	28
2	Methods	29
2.1	Schrödinger Equation	29
2.2	Born–Oppenheimer (BO) Approximation	30
2.3	Investigation of Many-electron Systems	31
2.4	Density Functional Theory	33
2.4.1	The Hohenberg-Kohn Theorems	33
2.4.2	Kohn-Sham Approach	36
2.4.3	Exchange and Correlation Functional	38
2.5	Other Approximations in Electronic Structure	39
2.5.1	Localized Basis Set	39
2.5.2	Mesh-Cutoff	39
2.5.3	Pseudopotential	40
2.6	Computational Details	41
2.6.1	SIESTA	41

3	Results	43
3.1	Two Dimensional Systems	43
3.2	Naphthylene- α Nanoribbons	45
3.2.1	Studied Structures	45
3.2.2	Electronic Band Structures and Local Density of States	49
3.2.3	Spin Polarization	53
3.3	Naphthylene- β Nanoribbons	57
3.3.1	Studied Structures	57
3.3.2	Electronic Band Structures and Local Density of States	59
3.3.3	Spin Polarization	62
4	Conclusions and Perspectives	66

Chapter 1

Literature Review

In this chapter, we present a literature review on graphene, graphene synthesis and some of the potential applications of this material. In addition, we discuss general features of other carbon allotropes that are relevant for our investigation. We also revise basic properties of graphene nanoribbons and other different two-dimensional nanocarbon systems, and how they motivated our work.

1.1 Carbon Based Materials

Carbon is one of the most abundant elements in nature. The different hybridizations allowed for carbon enable it to form distinct materials with a variety of dimensions, which is a feature strongly related to the electronic properties of the carbon atom [1].

A carbon atom has 6 electrons, which present the following electronic distribution $1s^2 2s^2 2p^2$. Electrons from $1s$ orbital are strongly bounded to the nucleus, and because of that, they are known as core electrons. The other four electrons are the valence electrons and they occupy the $2s$, $2p_x$, $2p_y$ and $2p_z$ orbitals. The wavefunction of these four electrons can superpose each other easily once the energy difference between the $2s$ and $2p$ orbitals is small when compared to the binding energy [2]. This process of mixing wavefunctions is called *hybridization*. The combination of s and p orbitals can form three different hybrid orbitals, which are sp , sp^2 and sp^3 . Firstly, when the hybridization occurs between a s and only one p orbital, it results in sp orbitals. As a consequence, the carbon atoms form two σ and two π bonds with the neighbors atoms. This kind of hybrid orbitals forms linear chains [2].

Regarding the sp^2 hybridization, it is a combination of one s orbital and two p orbitals, resulting in three in-plane hybrid orbitals, and consequently, planar structures are formed [2]. The three sp^2 hybridized orbitals make a 120° degree angle with each other. Graphene, for

example, presents sp^2 hybridization. Each atom is bounded to three other atoms forming σ bonds, and the out-of-plane p orbitals, which is not hybridized, form a π bond with the others out-of-plane p orbitals.

Lastly, sp^3 hybridization happens when a s orbital is combined with all three p orbitals, forming four σ bonds. In this mixing, the sp^3 orbitals make a $109^\circ28'$ angle with each neighbor orbital. The hybrid sp^3 orbitals give rise to tetrahedral structures [2], such as diamond and methane, for example.

Moreover, the absence of p orbitals in the core of carbon allows it to form more compact structures and with different structural arrangements. Figure 1.1 shows the structural representation of some allotropes of carbon, which have different hybridizations.

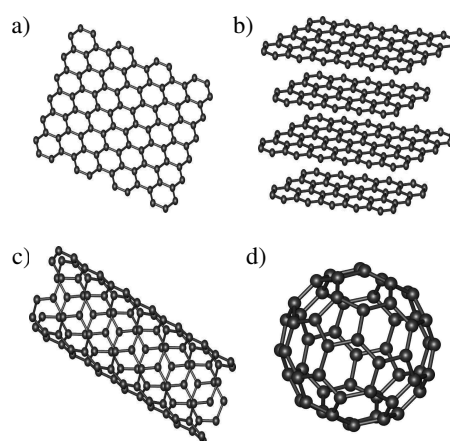


Fig. 1.1: Schematic representation of a) graphene, b) graphite, c) carbon nanotube, and d) fullerene, which are different allotropes of carbon.

In Fig. 1.1a we have the representation of graphene, a two-dimensional structure where the atoms are organized in a honeycomb lattice and have sp^2 hybridization. Figure 1.1b shows the structure of graphite, which is formed by the piling of layers of graphene that hold together due to van der Waals interactions. Those interactions are much weaker than the π and σ bonds inside a graphene sheet. Figure 1.1c is a representation of a single-wall carbon nanotube, a cylindrical structure of carbon atoms that can be pictured as a graphene sheet rolled up so as to form a tube. The discover of carbon nanotubes is often attributed to Iijima due to his paper published in 1991 [3]. However, in 1959, Roger Bacon produced images of carbon nanotubes, and in the 1980s, Howard Tennant applied for a patent on a method to produce this carbon-based material [4]. However, Iijima was the one who not only imaged carbon nanotubes in electron microscope but also explained what these structures really are, shedding light on the nanotube science [4]. Lastly, Fig. 1.1d displays a fullerene (C_{60}), structure also called buckyball,

which was discovered in 1985 [5, 6], but which has been predicted before, in 1970, by Ozawa [7, 8]. Fullerenes consist of hexagons and pentagons, what causes the formation of a spherical structure. Among those carbon allotropes, we will focus our attention on graphene and its physical properties.

1.2 Graphene

Graphene is a two-dimensional crystalline structure which was isolated in its few layered form in 2004 by Geim and Novoselov using the so-called mechanical exfoliation method [9, 10]. Their pioneering experiments regarding this 2D material rewarded them with the Nobel Prize in Physics in 2010. This material presents interesting and peculiar properties, such as high electronic mobility at room temperature [11], high flexibility [12], impermeability to gases [13], high electrical and thermal conductivity [14], among others [10]. All these properties together in a single material suggest that graphene has potential applications in areas related to composites, energy, electronics, environment and thin films, to quote a few [6]. Therefore, it has become a hot topic of interest for science and technology [9, 15]. In the following, we will discuss the structural and electronic properties of graphene, graphene synthesis and other potential graphene-based materials.

1.2.1 Structural Properties

Graphene is a one-atom thick two-dimensional allotrope of carbon. Its composing atoms are organized in a honeycomb lattice, thus forming hexagonal rings, as illustrated in Fig. 1.2.

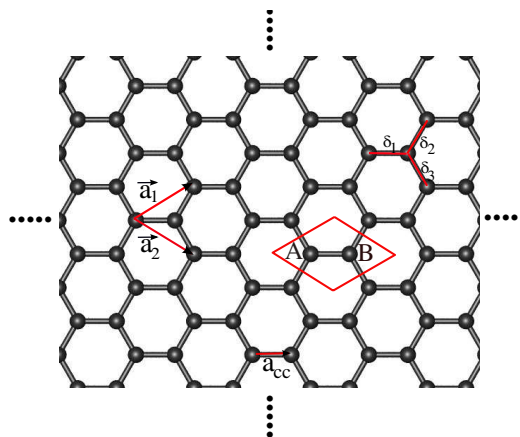


Fig. 1.2: Direct lattice of graphene.

The atomic structure of graphene can also be seen as a superposition of two triangular lattices, which we name as A and B sublattices. Differently from graphene, these two sublattices are now, separately, Bravais lattices. The a_{cc} parameter is the carbon-carbon bond length, which is about $0.142nm$. The δ_i ($i = 1, 2, 3$) vectors point to the three nearest neighbors of a carbon atom, and \vec{a}_1 and \vec{a}_2 are the primitive lattice vectors, which can be written as

$$\vec{a}_1 = \frac{a_{cc}}{2}(3, \sqrt{3}), \quad (1.1)$$

and

$$\vec{a}_2 = \frac{a_{cc}}{2}(3, -\sqrt{3}). \quad (1.2)$$

The corresponding reciprocal lattice, displayed in Fig. 1.3, is also a hexagonal lattice, however it is rotated by 30° relative to the direct lattice showed in Fig. 1.2.

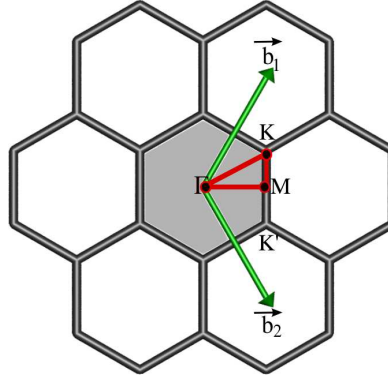


Fig. 1.3: Reciprocal lattice of graphene and its 1st Brillouin zone highlighted as gray.

The area in gray corresponds to the first Brillouin zone (BZ), which is the Wigner-Seitz cell of the reciprocal lattice. The Γ , K and M labels hold for the high symmetry points, where K and K' are also called the Dirac points. They can be written as follows

$$\Gamma = \frac{2\pi}{3a}(0, 0), \quad (1.3)$$

$$M = \frac{2\pi}{3a}(1, 0) \quad (1.4)$$

and

$$K = \frac{2\pi}{3a}\left(1, \frac{1}{\sqrt{3}}\right). \quad (1.5)$$

The reciprocal lattice has an important role in solid state physics, since the energy bands

are expressed as a function of the k points within the BZ. In addition, the interpretation and computation of many physical quantities require only the integration over the entire BZ [16]. In those integrations, one can use some properties, such as symmetry operations, so as to reduce the cost of computational calculations. This is why energy bands are usually expressed along the high symmetry points, which are the points on the boundary that define the irreducible Brillouin zone (IBZ). The IBZ is the smallest region of the BZ that is sufficient to express all the information on the excitations of the crystal [16]. The primitive vectors \vec{b}_1 and \vec{b}_2 of the reciprocal lattice can be written as follows

$$\vec{b}_1 = \frac{2\pi}{3a_{cc}}(1, \sqrt{3}), \quad (1.6)$$

$$\vec{b}_2 = \frac{2\pi}{3a_{cc}}(1, -\sqrt{3}). \quad (1.7)$$

Considering these vectors, it is possible to find the coordinates of the Γ , K and M points as showed in Equations 1.3, 1.4 and 1.5. If the BZ was not a regular polygon, we would have to do some calculations to find the coordinates of the high symmetry points.

1.2.2 Electronic Properties

Electronic structure (ES) theory describes how the electrons behave in a material, as well as it allows for the calculation of atomic forces, as a combination of interactions involving electrons and nuclei. These features determine the geometry and other physical properties of several stable structures. In short, ES deals with the ground and also excited states for electrons, their relation to the nuclear structure, and the spectroscopies connecting them [17]. The electronic structure of graphene and other nanomaterials can be understood as a relation between the energy and the wave vector in reciprocal space, which is usually called a dispersion relation. Figure 1.4 displays the electronic band structure of graphene over the whole Brillouin zone and along the high symmetry lines, respectively.

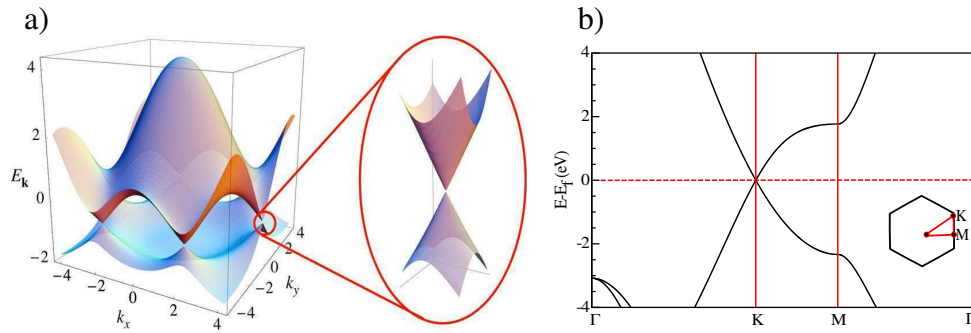


Fig. 1.4: a) Electronic band structure over the whole BZ (adapted from [18]) and b) along the high symmetry direction in the first Brillouin zone.

As mentioned before, graphene has sp^2 hybridization, what means that three of the valence electrons form σ bonds (in-plane) and the remaining one forms a single π bond (out of the plane). Since the latter one forms a weaker bond, it is responsible for most of the electronic properties around the Fermi level [18]. The points where the valence and conduction bands touch each other are called Dirac points. For this reason, graphene is known as a zero gap semiconductor. These points are located at the vertices of the BZ (K and K' points). Due to the linear dispersion at these points, electrons in graphene behave as massless particles and obey Dirac equation [19]. Therefore, electrons in graphene have a high mobility ($200.000 \text{ cm}^2/\text{V.s}$) [20], which is 100 faster than in silicon ($1400 \text{ cm}^2/\text{V.s}$), for example.

Even though graphene features all these interesting properties, it is still a zero gap semiconductor. In gapless materials, it is not possible to control the behavior of electrons, what is a required feature in nanoelectronic applications. Therefore, many strategies have been proposed to open a tunable band gap in this material. For instance, we can mention the introduction of structural defects [21], chemical doping [22] and the reduction of dimensionality, such as in graphene nanoribbons [23] (which are one-dimensional graphene nanostrips). Another mechanism that has been investigated by the scientific community is the reorganization of atoms so as to form materials still made of carbon atoms, but not arranged in a honeycomb lattice. For example, graphenylene, which is a sp^2 -carbon structure composed of cyclohexatriene units with two quite distinct C–C bonds within a C6 ring [24], is a 2D lattice presenting a tiny electronic band gap.

1.2.3 Graphene Synthesis

Even though graphene was isolated by mechanical exfoliation, there are other different techniques able to produce this 2D material. Chemical Vapor Deposition-CVD [25] and epitaxial

growth [26] are representative examples. However, in order to introduce this material in industry, it is needed a large-scale production route which not only maintains all those peculiar properties of graphene, but also solves some issues related to it, such as the zero gap feature. Several methods to fabricate graphene have been reported and they can be divided into two different approaches: top-down and bottom-up, as illustrated in Fig. 1.5 below.

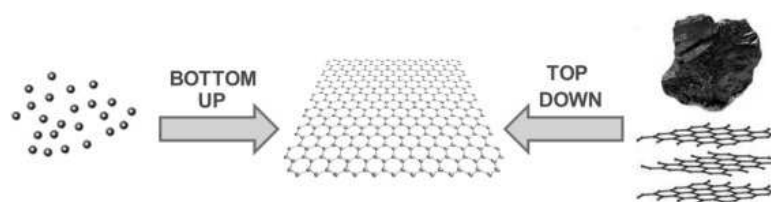


Fig. 1.5: Schematic representation of bottom-up and top-down approaches. Adapted from [27].

An example of a Top-down approach is the separation of the graphite layers, thus yielding single graphene sheets [28]. The basic idea of a top-down technique is starting from a larger bulk structure in a way to obtain a smaller system. By using this approach, one can have high control of placement and location of the produced material. However, there are also disadvantages, such as the damage of the layers while separating them, finite source of graphite, possibility of reagglomeration of the layers during the exfoliation process and also it takes numerous steps to go from graphite to graphene layers. Some methods that use this approach are: *micromechanical cleavage*, *electrochemical exfoliation*, *exfoliation of graphite by intercalating compounds*, *solvent-based exfoliation* and *unzipping of carbon nanotubes* [28]. Fig. 1.6 shows images of carbon nanoparticles, carbon nanoribbons and graphene sheets produced by electrochemical exfoliation, for example [29, 30].

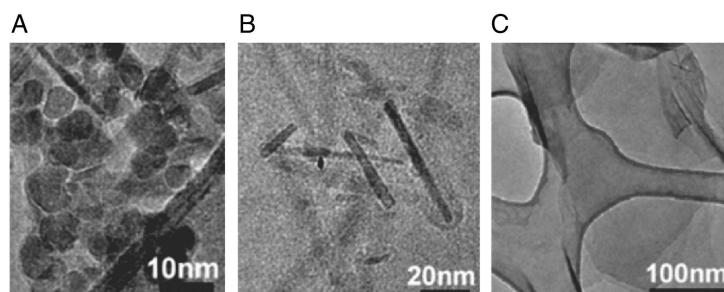


Fig. 1.6: (a) Transmission electron microscopy (TEM) image of carbon nanoparticles, (b) carbon nanoribbons and (c) graphene sheets produced by electrochemical exfoliation [29, 30].

On the other hand, for bottom-up approaches, they promote high levels of graphitisation, thus producing good materials, what usually requires high temperatures [28]. The basic idea is starting from atoms or molecules in a way to obtain a larger system. Bottom-up methods present high control of resolution [31], and they are usually simpler than top-down methods. Bottom-up techniques enable the production of graphene nanoribbons and nanoflakes since one of the biggest advantages of these techniques is the control of resolution, what guarantees precision at the atomic-level [31]. Some bottom-up methods are, for example, *epitaxial growth on silicon carbide*, *chemical vapor deposition (growth on metal, substrate free)*, *surface assisted reactions and miscellaneous methods* [28]. As an example of one of these techniques, Fig. 1.7 displays images of graphene films grown by CVD.

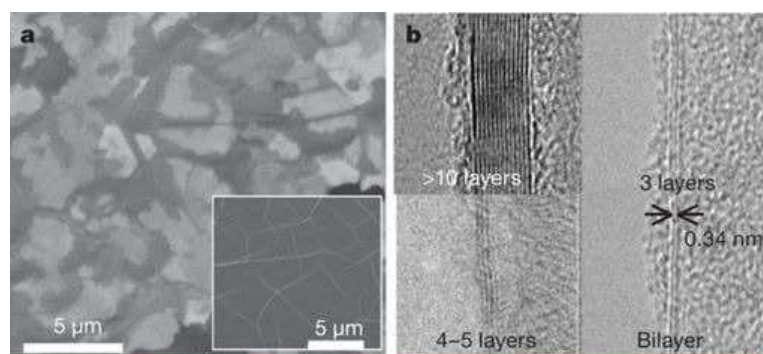


Fig. 1.7: a) Scanning electron microscopy (SEM) images of grown graphene films on thin (300-nm) nickel layers and thick (1-mm) Ni foils (inset). b) TEM images of graphene films of different thicknesses [32].

As far as it is known, all methods reported to produce graphene have advantages and disadvantages. Therefore, the final choice has to be conducted by the final application of this material [28].

1.2.4 Potentialities for Graphene-based Materials

Graphene and its related systems are versatile materials, as a consequence of their interesting optical, mechanical and electrical properties. As a result, their use has been considered and studied in many areas. Due to its transparency and flexibility, for example, graphene has become a potential material for electrodes. Touch-screen sensors [12], organic light-emitting diodes [33], and organic photovoltaic devices [34] are some examples of flexible devices using graphene as a transparent electrode. However, integrating graphene-based transparent electrodes into commercial devices in large-scale production, with low-cost and good quality, is still

a challenge [35].

Another area that graphene has gained some attention is on energy storage. A device that could possess both high energy and high power would be a very good option to enhance some issues related to electrochemical capacitors and batteries, for example [35]. Once graphene presents a high surface area and high electrical conductivity, it has become a very attractive material to this end [36]. However, probably it is too early to say when and whether or not graphene will replace traditional materials in batteries and capacitors, since many challenges still have to be overcome, such as thickness, uniformity, particle sizes, purity and surface area [35].

Graphene has also attracted great attention in the semiconductor field as silicon-based devices approach their limit of miniaturization and improvements of performance [37]. However, instead of replacing silicon completely, graphene is more likely to be used to improve silicon-based electronics [37].

Graphene-based sensors have been another topic of intense research [10]. Since graphene is, at the same time, a sensing and conducting surface, it can exhibit a very high sensitivity [35]. In traditional sensors, these two features are separated [38]. Related to medical topics, graphene has also been considered as a candidate to the production of artificial implants and tissue components, such as orthopedic implants [39]. It is important to stress that even though there is intense research in the area, biomedical applications of graphene are in early stages of development [35]. The future of graphene-based materials and their applications is difficult to predict, but it is likely they will have a very important role in different areas.

Considering the possibility to open a band gap in graphene, other systems are proposed to investigate how their electronic properties behave. Therefore, the two next sections are about graphene nanoribbons and unusual two-dimensional graphene-like materials, respectively.

1.3 Graphene Nanoribbons

In order to open a band gap in graphene, an alternative is to work with one dimensional periodic nanostrips of graphene, which are commonly called *graphene nanoribbons*. One can “cut” graphene nanoribbons along two high-symmetric directions in graphene, as shown in Fig. 1.8, consequently producing graphene nanoribbons with *zigzag* and *armchair* edges. Even though we are going to focus on these two types of nanoribbons, there are also graphene nanoribbons with *chiral* edge orientation, what means that zigzag and armchair segments alternate periodically along the edges [40].

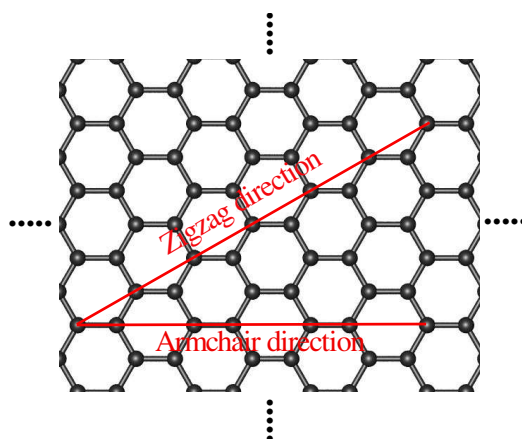


Fig. 1.8: Directions of high symmetry in graphene.

The atomic structure of zigzag and armchair graphene nanoribbons are represented in Fig. 1.9. The zigzag nanoribbons are classified according to the number of zigzag chains across the ribbon width and the armchair nanoribbons according to the number of dimer lines across the ribbon width. Usually, graphene nanoribbons have edges saturated by hydrogen atoms. In Fig. 1.9 we show a 10-ZGNR and a 10-AGNR, respectively.

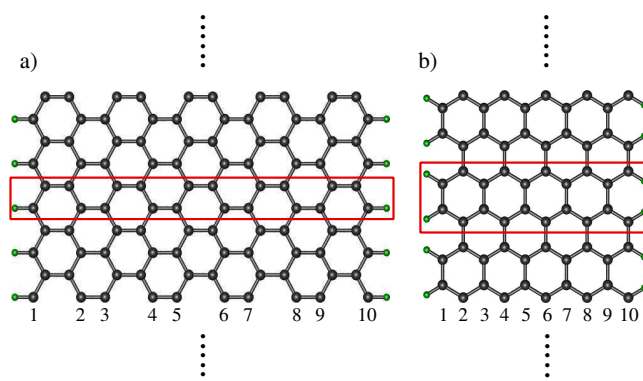


Fig. 1.9: Atomic structure of a) zigzag and b) armchair graphene nanoribbons. The boxes in red highlight the unit cell of each nanoribbon.

The electronic band structure of zigzag and armchair graphene nanoribbons are quite different [15]. The electronic levels also depend on other features, such as the width and the spin polarization of their edges. In Fig. 1.10 we have the electronic band structure of a 10-ZGNR (zigzag graphene nanoribbon with 10 zigzag chains across the ribbon width) and of a 10-AGNR (10 dimer lines across the ribbon width), respectively, obtained by performing calculations using the same methodology described in chapter 2.

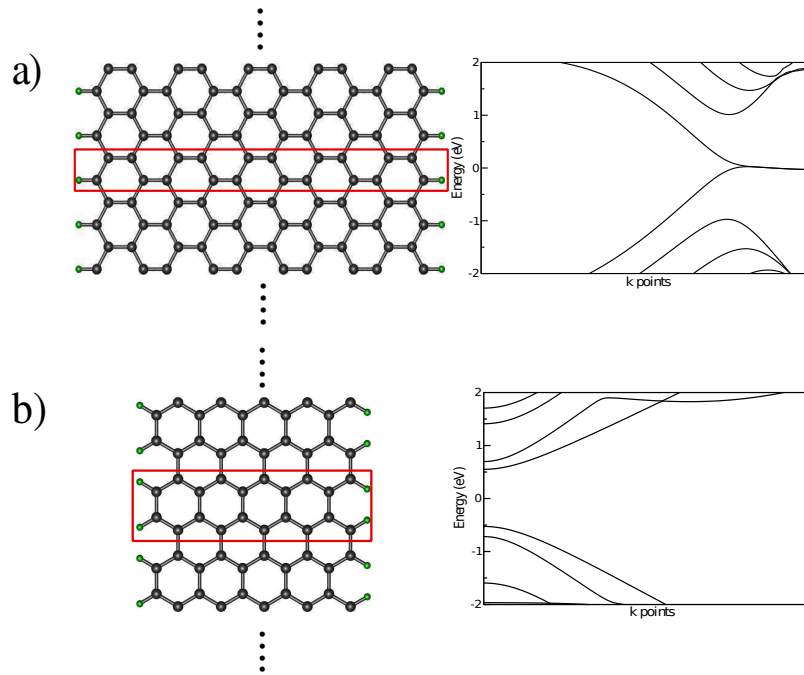


Fig. 1.10: Atomic structure of a) zigzag graphene nanoribbon and b) armchair graphene nanoribbon along with their electronic band structures. The boxes in red highlight the unit cell.

The band structures of these two types of nanoribbons are very distinct. For the zigzag nanoribbon, there is a flat band at the Fermi level, and this metallic behavior does not depend on the ribbon width [41, 42]. Therefore, ZGNRs always show localized states at the Fermi level when we do not take spin polarization explicitly into account. This suggests a magnetic ordering [15]. As discussed by Pisani *et al* in [41], there is an instability associated to this high density of states at the Fermi level. In order to solve this instability, the system spontaneously shows spin polarization along the edges, since other alternatives such as geometric distortion do not show preferable to stabilize the system successfully [41]. In the same work, it is investigated two types of spin polarization. The antiferromagnetic (AFM) configuration, where the spin moments on the atoms on one edge are antialigned to the spin moments on the opposite edge, and the ferromagnetic (FM) configuration, where the spin moments on both edges have the same orientation [41]. Figure 1.11 shows the electronic band structure of a 10-ZGNR with AFM and FM spin orientations, respectively. These bands also were obtained by means of the methods described in the following chapter.

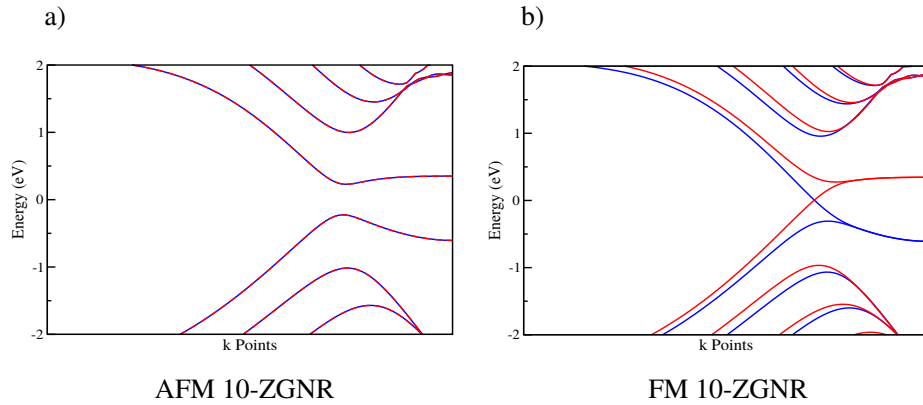


Fig. 1.11: Electronic band structure of zigzag graphene nanoribbon a) with AFM orientation and b) FM orientation.

As we can see, the AFM configuration shows a band gap around the Fermi energy, while in the FM configuration, the nanoribbon shows a metallic behavior. The blue (red) bands represent spin up (down) electronic states. In addition, the AFM configuration is more stable than the non polarized and the FM configuration [1].

Armchair graphene nanoribbons are predicted to be either semiconductor or metallic. These two features depend directly on the nanoribbon width [15]. AGNRs can be divided into 3 different families: those with $3p$, $3p + 1$ and $3p + 2$ rows of dimers across their width [23], where p is a positive integer. These families of ribbons and the variation in their band gap as a function of the ribbon width are displayed in Fig. 1.12.

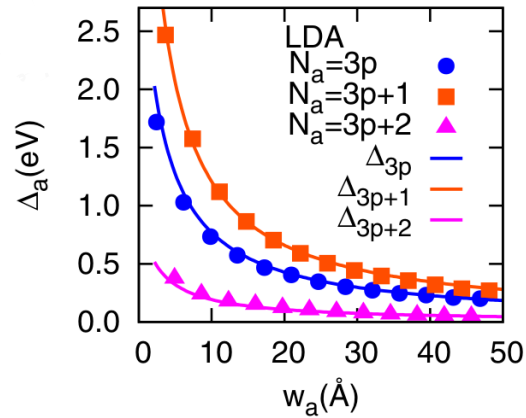


Fig. 1.12: Variation of the band gaps of AGNRs as a function of the ribbon width (W_a). Adapted from [42].

For these 3 families of armchair nanoribbons, we can state that $\Delta_{3p+1} \geq \Delta_{3p} \geq \Delta_{3p+2}$ and for each of these families, the band gap decreases with increasing ribbon width [42].

1.4 Two-dimensional Carbon Networks

The lack of band gap in graphene has motivated the investigation of many two-dimensional materials [43], such as graphenylene [24, 44], phagraphene [45], amorphized graphene [46], biphenylene [47], Haecklites [48, 49] etc. Since the atomic structures of these materials are directly related to their physical properties, it is needed a deep understanding of the relationship between these two features. Fig. 1.13 shows, for example, the atomic structure of biphenylene, amorphous graphene and phagraphene, respectively.

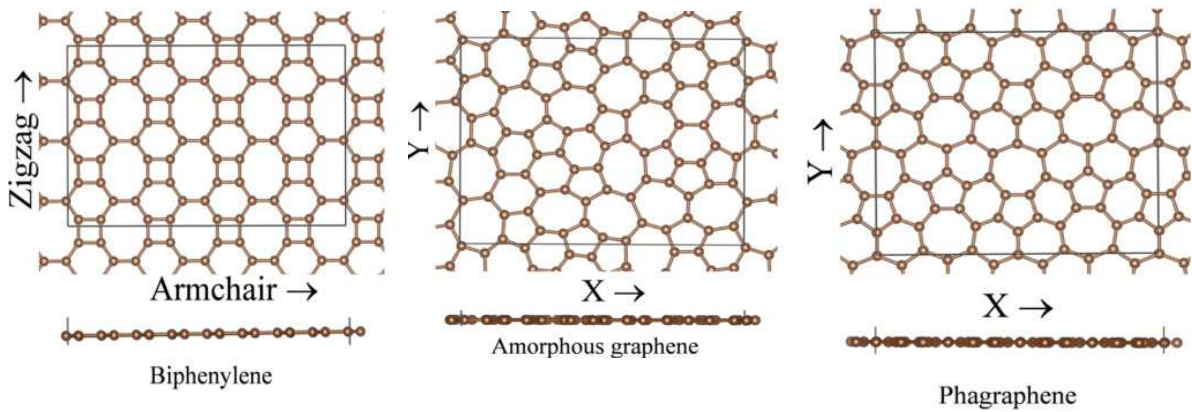


Fig. 1.13: Atomic structure of biphenylene, amorphous graphene and phagraphene. Adapted from [43].

As we can see, like graphene, these networks are still two-dimensional, but the arrangements of their atoms are different from a honeycomb lattice. Among this variety of graphene-like systems, we will focus our attention on graphenylene, which motivated this dissertation.

Graphenylene, firstly proposed by Balaban and Vollhardt [24], is a hypothetical two dimensional sp^2 -carbon structure constituted by 4, 6 and 12-membered rings in a triangular lattice, as in graphene. However, the lattice parameters of graphenylene are $a=b=6.76 \text{ \AA}$, and its unit cell contains 12 sp^2 -hybridized carbon atoms. The Brillouin zone of this material is similar to that of graphene, namely a regular hexagon. Figures 1.14a and 1.14b represent the atomic structure and the electronic band structure of graphenylene, respectively.

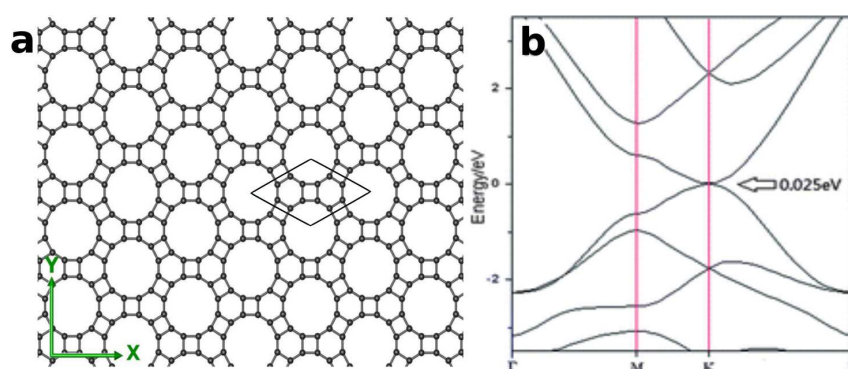


Fig. 1.14: a) Atomic structure of graphenylene along with b) its electronic band structure [24].

First-principles calculations on this network predict a narrow direct band gap (0.025 eV) [24]. Even though energetically less favourable than graphite and diamond, for example, graphenylene is thermodynamically more stable than graphyne and carbyne [24]. In addition, its phonon dispersion curves showed that there are no imaginary frequencies [24]. All these results indicate that graphenylene is a sp^2 -hybridized carbon allotrope able to exist in reality [24]. These structures can also be thought as cut into nanoribbons. Figure 1.15 displays the electronic band structures of two types of graphenylene nanoribbons proposed by Qi Song *et al* [24], which also exhibit a direct band gap around the Fermi level, but much larger than that of graphenylene.

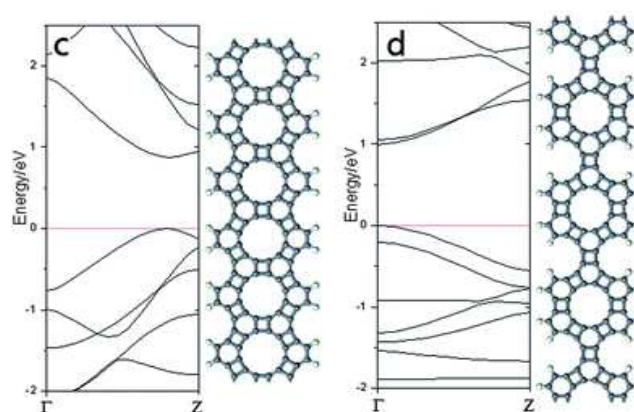


Fig. 1.15: c) electronic band structure of graphenylene nanoribbon with zigzag edge and d) armchair edge, respectively. Adapted from [24].

One potential application of graphenylene is on the separation of H_2 molecule from other gases, such as CO [24]. This is due to the fact that the pore diameter (3.2 Å) is larger than H_2 molecules, thus enabling a separation from molecules larger than the pore diameter (like the case of CO) [50].

1.5 This Work

Considering the idea of sp^2 -carbon systems with a structural unit different from that of graphene, such as graphenylene, we propose in this work a new 2D-system where the structural unit is a naphthyl group, which is shown in Fig 1.16b. According to the way these naphthyl units are arranged in the structure, we can have two different 2D networks. We named the first one as naphthylene- α , and the second one as naphthylene- β . The way the naphthyl units are arranged in naphthylene- α structure is similar to the cyclic 3-naphthylene presented by Balaban and Vollhardt in [51].

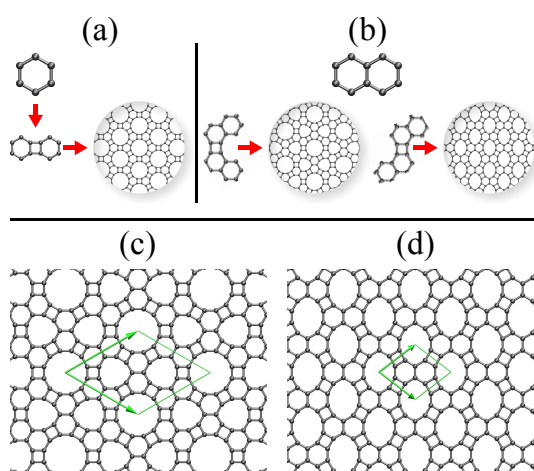


Fig. 1.16: Basic building block of a) graphenylene and b) naphthylene- α and naphthylene- β systems, c) naphthylene- α sheet, d) naphthylene- β sheet.

We also investigated, by means of computational methods, the electronic properties of possible nanoribbons that can be *constructed* from these 2D-systems. A way to construct precise nanoribbons of different topologies and widths, for instance, is to use surface-assisted reactions [52]. Cai *et al* [52], for example, show that using different molecules, 10,10'-dibromo-9,9'-bianthryl and 6,11-dibromo-1,2,3,4-tetraphenyltriphenylene, in a surface-assisted reaction generates straight armchair edged or wigglylike ribbon, respectively [53].

In the next chapter, the methodology used to perform the calculations of the electronic structure of the proposed systems is presented and discussed. In chapter 3, we show the atomic structure of all systems studied and the results obtained regarding their electronic properties. Lastly, in chapter 4, we present the conclusions that arised from this work.

Chapter 2

Methods

In this chapter we present and discuss the methods and approximations used to compute the electronic structure for the systems studied in this work.

2.1 Schrödinger Equation

In order to describe the electronic structure of matter, we have to rely on theoretical concepts and methods of quantum mechanics. Therefore, we can start with the time-independent Schrödinger equation, which governs a non-relativistic quantum system. It is written as

$$E\psi = \hat{H}\psi, \quad (2.1)$$

where \hat{H} is the Hamiltonian, E represents the energy eigenvalues and ψ are the eigenfunctions of the system.

The Hamiltonian \hat{H} for a system that consists of nuclei (upper case subscripts) and electrons (lower case subscripts) can be written (in atomic units) as

$$\hat{H} = -\frac{1}{2} \sum_i \nabla_i^2 - \sum_{i,I} \frac{Z_I}{|\mathbf{r}_i - \mathbf{R}_I|} + \sum_{i \neq j} \frac{1}{|\mathbf{r}_i - \mathbf{r}_j|} - \sum_I \frac{1}{2M_I} \nabla_I^2 + \sum_{i \neq j} \frac{Z_i Z_j}{|\mathbf{R}_I - \mathbf{R}_J|}, \quad (2.2)$$

or summarized as

$$\hat{H} = \hat{T}_e + \hat{V}_{e-n} + \hat{V}_{e-e} + \hat{T}_n + \hat{V}_{n-n}, \quad (2.3)$$

where \hat{T}_e and \hat{T}_n are the kinetic energy operators for electrons and nuclei, respectively, \hat{V}_{e-n} represents the potential energy between electrons and nuclei, \hat{V}_{e-e} is the potential energy from

electron–electron repulsions, and \hat{V}_{n-n} denotes the potential energy from nuclei–nuclei repulsions. The electron–electron interaction, expressed by \hat{V}_{e-e} , is a very difficult term to deal with, reason for what the analytical solution to a many-body system is not known. Therefore, the main problem of electronic structure is to develop mechanisms to approach electronic correlations, enabling one to predict and study the different phenomena displayed by matter at the nanoscale.

Another issue, when solving the many body problem for molecular systems, is the coupling between the electronic and nuclear parts of the problem. A first approximation to work with this difficulty is to assume that the Schrödinger equation can be solved separately for electrons and nuclei. This simplification is provided by *the Born–Oppenheimer approximation* [54], which is discussed in the next section.

2.2 Born–Oppenheimer (BO) Approximation

Considering the Hamiltonian \hat{H} for the Schrödinger equation (Eq. 2.2), we will not be able to find the analytical solution. The term \hat{V}_{e-n} involves electrons and nuclei, what makes Eq. 2.2 a non-separable equation. Aiming to decouple the electronic motion from the nuclear motion, we introduce the Born–Oppenheimer approximation [54], which finds physical reason in the fact that the nuclei are very heavy in comparison to the electrons. For this reason, the nuclei behave as if they were nearly fixed with respect to the electronic motion. The final consequence is that the motion of electrons and nuclei can be solved separately. It can be shown that this separation yields wavefunctions that can be expressed as a product of two functions, that is

$$\Psi(\mathbf{r}_i, \mathbf{R}_I) = \psi_R(\mathbf{r}_i) \cdot \mathcal{X}(\mathbf{R}_I), \quad (2.4)$$

where $\psi_R(\mathbf{r}_i)$ is the electronic wavefunction, which also depends on nuclear positions, and $\mathcal{X}(\mathbf{R}_I)$ is the nuclear wavefunction.

It can be shown that $\psi_R(\mathbf{r})$ satisfies the following Schrödinger equation

$$[\hat{T}_e + \hat{V}_{e-n} + \hat{V}_{e-e}] \psi_R(\mathbf{r}_i) = U(\mathbf{R}_I) \psi_R(\mathbf{r}_i), \quad (2.5)$$

which describes only the electronic part of the system. Commonly, the $\hat{H}_e = \hat{T}_e + \hat{V}_{e-n} + \hat{V}_{e-e}$ operator is called electronic Hamiltonian. For each nuclear configuration, $U(\mathbf{R}_I)$ is part of a set of eigenvalues for different electronic states.

Considering Eq. 2.1, Eq. 2.4 and Eq. 2.5, we obtain the equation for the nuclear part of the problem as

$$\left(-\sum_I \frac{\hbar^2}{2M_I} \nabla_I^2 + U(\mathbf{R}_I)\right)\Psi(\mathbf{r}_i, \mathbf{R}_I) = E\Psi(\mathbf{r}_i, \mathbf{R}_I). \quad (2.6)$$

Rewriting Eq. 2.6 above, we have

$$\left(-\sum_I \frac{\hbar^2}{2M_I} \nabla_I^2 + U(\mathbf{R}_I)\right)\mathcal{X}(\mathbf{R}_I) = E\mathcal{X}(\mathbf{R}_I), \quad (2.7)$$

describing, thus, the nuclei motion separated from the electronic motion. In the following, the search for electronic molecular orbitals is done considering different methods. In ab initio molecular dynamics, the nuclear problem is usually replaced by an integration of Newton's equations, considering the electronic energy as part of an effective potential [55]. Even using the Born-Oppenheimer approximation, the Schrödinger equation can only be solved exactly for one-electron systems. In order to apply it to a system of many electrons, one must evaluate the difficulties and try to reach at least approximated solutions, as discussed in the next sections.

2.3 Investigation of Many-electron Systems

Aiming to solve the electronic Schrödinger equation that was elaborated after using the Born-Oppenheimer approximation, different methods have been developed. The first consideration about the many electron problem is that the electrons are interacting particles. Thus, a first approximation that can be made is to consider that electrons are independent particles in an effective potential. Therefore, one possibility is to consider that the wavefunction of the system can be written as a product of one-electron orbitals,

$$\Psi(\mathbf{x}_1, \mathbf{x}_2, \dots, \mathbf{x}_n) = \phi_1(\mathbf{x}_1)\phi_2(\mathbf{x}_2)\dots\phi_n(\mathbf{x}_n). \quad (2.8)$$

This approach, proposed by Hartree in 1928, considers that the potential felt by an electron was due to the field created by the cloud of the remaining electrons together with the potential of the nuclei, and a two-body interaction assumes the classical electrostatic form [55].

In general, theories of non-interacting particles have an effective potential that takes into account some effects of the real interaction. This is cast in the following Schrödinger like equation,

$$\hat{H}_{eff}^i \Psi_i(\mathbf{r}) = \left[-\frac{\hbar^2}{2m_e} \nabla^2 + V_{eff}^\sigma(\mathbf{r}) \right] \Psi_i^\sigma(\mathbf{r}). \quad (2.9)$$

In this case, the effective potential $V_{eff}^\sigma(\mathbf{r})$ acting on each electron of spin σ at \mathbf{r} and can be

expressed as

$$V_{eff}^\sigma = V_{ext}(\mathbf{r}) + V_{Hartree}(\mathbf{r}). \quad (2.10)$$

The second term in Eq. 2.10 is the classical electrostatic potential felt by a particle due to the electronic density from all the other electrons, also called Hartree potential.

Electrons are indistinguishable fermions, what means that when two electrons are exchanged, the wavefunction must change sign, i.e., it has to be antisymmetric (condition not satisfied by Eq. 2.8). Once the Hartree approach does not include this property, the description of the electronic problem asks for a more complete procedure.

Therefore, the next step is to take into account the antisymmetry of the wavefunction. In order to account for this aspect, it was proposed an approximation for the antisymmetrized many electron wavefunction in the form of a Slater determinant [56], as shown below

$$\Psi(\mathbf{x}_1, \mathbf{x}_2, \dots, \mathbf{x}_n) = \frac{1}{\sqrt{N!}} \begin{bmatrix} \phi_1(\mathbf{x}_1) & \phi_1(\mathbf{x}_2) & \dots & \phi_1(\mathbf{x}_n) \\ \phi_2(\mathbf{x}_1) & \phi_2(\mathbf{x}_2) & \dots & \phi_2(\mathbf{x}_n) \\ \vdots & \vdots & \ddots & \vdots \\ \phi_n(\mathbf{x}_1) & \phi_n(\mathbf{x}_2) & \dots & \phi_n(\mathbf{x}_n) \end{bmatrix}$$

where $\phi_i(\mathbf{x}_1)$ represents the i th one-electron spin orbital (spatial and spin component), and (j) refers to the spatial and spin coordinate of electron j . This procedure results in the so called Hartree-Fock (HF) approximation, and it introduces the concept of particle exchange energy [57, 58]. We end up with a Schrödinger equation analogous to Eq. 2.9, except by the fact that the effective Hamiltonian depends on the state. This can be written as follows,

$$\hat{H}_{eff}^i \Psi_i(\mathbf{r}) = \left[-\frac{\hbar^2}{2m_e} \nabla^2 + V_{eff}^{i,\sigma}(\mathbf{r}) \right] \Psi_i^\sigma(\mathbf{r}), \quad (2.11)$$

where

$$V_{eff}^{i,\sigma} = V_{ext}(\mathbf{r}) + V_{Hartree}(\mathbf{r}) + \hat{V}_x^{i,\sigma}(\mathbf{r}), \quad (2.12)$$

and the exchange potential $\hat{V}_x^{i,\sigma}(\mathbf{r})$ is a sum over orbitals of the same spin σ [16], written as

$$V_x^{\hat{i},\sigma}(\mathbf{r}) = - \left[\sum_j \int dr' \Psi_j^{\sigma*}(\mathbf{r}') \Psi_i^\sigma(\mathbf{r}') \frac{1}{|\mathbf{r} - \mathbf{r}'|} \right] \frac{\Psi_j^\sigma(\mathbf{r})}{\Psi_i^\sigma(\mathbf{r})}. \quad (2.13)$$

The Hartree-Fock approximation has been used for a long time as a way to calculate the electronic structure of different systems. Even though it gives a reasonable picture of the atomic system, the Slater determinant does not describe exactly the wavefunction of a many

electron system. In this approach, all correlations, except those required by the exclusion Pauli's principle, are neglected [16]. The term that is not included in the HF approximation is the electronic correlation.

In the following section, it is discussed another method to approach the many body problem that takes into account not only the exchange but also the correlation effects.

2.4 Density Functional Theory

In quantum mechanics, complete information concerning the state of a system (atom, molecule or solid) is contained in the wavefunction, determined by the Schrödinger equation. However, in 1964, Hohenberg and Kohn proposed a new way of writing and solving quantum problems based not only on the wavefunction, but on the ground state electron density [59, 60]. This is the proposal of Density Functional Theory (DFT), which offers a strategy to solve the electronic problem of many body systems from the knowledge of the ground state electron density, as all the Hamiltonian terms describing the system can be written as functionals of this density. A functional is nothing more than a rule which assigns a number to a function. Therefore, while the density is a function with three variables (position of the electrons), the wavefunction is a function with $3N$ variables, which is much more complex to solve. Unlike other theories addressing the problem of many bodies, DFT is, in principle, an exact theory, although approximations have to be made in the practical implementation of this method. This theory is based on the Hohenberg-Kohn theorems and the Kohn-sham equations, which we will discuss in the following.

2.4.1 The Hohenberg-Kohn Theorems

The two theorems announced by Hohenberg and Kohn in 1964 serve as pillars of DFT [60] and show that from the ground state electron density, it is possible to obtain the ground state energy exactly. For the first theorem, we have

1° **Theorem:** *From the ground state density $\rho_0(r)$, one can unambiguously determine, to within a constant, the external potential $V_{ext}(r)$ of a system composed of many electrons.*

In order to prove this theorem, we can start by supposing that there are two external potentials, $V_{ext}(r)$ and $V'_{ext}(r)$, that differ from each other by more than a constant and that originate from the same ground state density $\rho_0(r)$. These different potentials determine two

Hamiltonians H and H' , which provide two wavefunctions ψ_0 and ψ'_0 for their respective ground states. According to this assumption, the Hamiltonians differ only by the external potential,

$$H = T + V_{ee} + V_{ext} \quad (2.14)$$

and

$$H' = T + V_{ee} + V'_{ext}. \quad (2.15)$$

We systematically have

$$V_{ext} \Rightarrow H \Rightarrow \psi_0 \Rightarrow \rho_0(r) \Leftarrow \psi'_0 \Leftarrow H' \Leftarrow V'_{ext}. \quad (2.16)$$

Using the variational principle, we can write

$$\langle \psi_0 | H | \psi_0 \rangle = E_0 < \langle \psi'_0 | H | \psi'_0 \rangle = \langle \psi'_0 | H' | \psi'_0 \rangle + \langle \psi'_0 | H - H' | \psi'_0 \rangle \quad (2.17)$$

$$E_0 < E'_0 + \int \rho_0(r)(V_{ext} - V'_{ext})dr. \quad (2.18)$$

In the same sense, we have

$$\langle \psi'_0 | H' | \psi'_0 \rangle = E'_0 < \langle \psi_0 | H' | \psi_0 \rangle = \langle \psi_0 | H | \psi_0 \rangle + \langle \psi_0 | H' - H | \psi_0 \rangle \quad (2.19)$$

$$E'_0 < E_0 - \int \rho_0(r)(V'_{ext} - V_{ext})dr. \quad (2.20)$$

Adding these two equations, we obtain

$$E_0 + E'_0 < E'_0 + E_0. \quad (2.21)$$

The equation above (Eq. 2.21) shows that if we consider two distinct external potentials V_{ext} and V'_{ext} yielding the same ground state density, $\rho_0(r)$, we arrive at a contradiction, which confirms that the external potential is univocally determined by the ground state electron density [59].

We can write the energy as a functional of the electron density by means of

$$E[\rho(r)] = T[\rho(r)] + E_{ee}[\rho(r)] + E_{ext}[\rho(r)], \quad (2.22)$$

where $T[\rho(r)]$ represents the kinetic energy, $E_{ee}[\rho(r)]$ the electron-electron interaction energy, and $E_{ext}[\rho(r)]$ includes the nuclei-electron interaction energy and the other contributions from external fields. By separating terms that are system independent ($T[\rho(r)]$ and $E_{ee}[\rho(r)]$) from those that are system dependent, we can rewrite Eq. 2.19 as

$$E[\rho(r)] = \int \rho(r)V_{ext}dr + T[\rho(r)] + E_{ee}[\rho(r)], \quad (2.23)$$

or

$$E[\rho(r)] = \int \rho(r)V_{ext}d^3r + F_{HK}[\rho(r)]. \quad (2.24)$$

here, F_{HK} is the sum of the kinetic energy and the electron-electron interaction and it is a universal functional. The second theorem can be stated as follows:

2° Theorem : *A universal functional for the energy in terms of the density can be defined and the ground state electron density is that which minimizes the energy, and this minimum value E_0 corresponds to the ground state energy $E[\rho_0(r)]$.*

In order to prove the second theorem, we consider that

$$E_{HK}[\rho(r)] = F_{HK}[\rho(r)] + \int \rho(r)V_{ext}d^3r, \quad (2.25)$$

where we now call the energy functional as E_{HK} . Now consider a system with the ground state density equal to $\rho_0(r)$, so that

$$E_0 = E_{HK}(\rho_0) = \langle \psi_0 | H | \psi_0 \rangle. \quad (2.26)$$

Considering another density $\rho_1(r)$, which does not correspond to that of the ground state, we have

$$E_0 = E_{HK}(\rho_0) = \langle \psi_0 | H | \psi_0 \rangle < \langle \psi_1 | H | \psi_1 \rangle = E_1 = E_{HK}(\rho_1). \quad (2.27)$$

Therefore, for any density other than the ground state density, there is a corresponding wave-function, ψ , which acting on the Hamiltonian of the system will return an energy value greater than the ground state energy, that is, the energy is minimized by the ground state electron density [59].

From these two theorems, we have seen that all the properties of a system can be determined

by the ground state electron density.

The Hohenberg-Kohn theorems propose the exact solution of the many body problem from the ground state density. However, they do not provide a practical procedure for the use of the functionals in order to find the ground state electron density. In 1965, Kohn and Sham suggested an approach to this problem and contributed heavily to DFT as we know and use today.

2.4.2 Kohn-Sham Approach

Kohn and Sham proposed a fictitious system of non-interacting electrons with the same electronic density of the real system [61]. However, the kinetic energy of this system is different from the kinetic energy of the actual system, even though they have the same electronic density.

In order to obtain the kinetic energy of the auxiliary system, as proposed by KS, we have to write

$$T_{KS} = -\frac{1}{2} \sum_1^N \langle \psi_i | \nabla^2 | \psi_i \rangle, \quad (2.28)$$

where ψ_i , which are the one-electron wavefunctions, must be written in terms of a basis in order to conduct the calculations. The use of a set of basis functions for the eigenfunction expansion allows one to write the problem in terms of matricial equations. In this case, one option is to use orbital-like wavefunctions as basis functions, as we discuss later.

For the universal functional, we can write

$$F[\rho(r)] = T_{KS}[\rho(r)] + J[\rho(r)] + E_{xc}[\rho(r)], \quad (2.29)$$

where $J[\rho(r)]$ represents the classical Coulomb interaction and $E_{xc}[\rho(r)]$ is the exchange-correlation energy, which represents the portion of the kinetic energy that can not be included in T_{KS} , as well as all the contributions of the electron-electron interaction other than $J[\rho(r)]$. Moreover, the $E_{xc}[\rho(r)]$ term takes into account all many-body effects of exchange and correlation, and it can be written as [16]

$$E_{xc}[\rho] = (T[\rho] - T_{KS}) + (E_{ee}[\rho] - J[\rho]). \quad (2.30)$$

Therefore, the exchange-correlation energy $E_{xc}[\rho]$ is the difference between the kinetic energy of the auxiliary system and the kinetic energy of the real system, plus non-classical electrostatic contributions, including the exchange and correlation term [60]. Thus, in this auxiliary system,

all the complexity of the many body system is included on the exchange-correlation functional, that is, when solving the system of equations proposed by Kohn-Sham. Therefore, the accuracy of the results is limited by this functional [60].

Regarding the Kohn-Sham Hamiltonian, we have

$$\hat{H}_{eff}^i(\mathbf{r}) = -\frac{1}{2}\nabla^2 + V_{KS}^\sigma(\mathbf{r}), \quad (2.31)$$

with

$$V_{KS}^\sigma(\mathbf{r}) = V_{ext}(\mathbf{r}) + V_{Hartree}(\mathbf{r}) + V_{xc}(\mathbf{r}), \quad (2.32)$$

where the only unknown term is the exchange-correlation potential $V_{xc}(\mathbf{r})$. The form of this potential can be deduced by the use of the 2nd HK theorem using the density ρ as written from the wavefunction of the auxiliary system.

Unlike the Hartree-Fock model, the Kohn-Sham approach to density functional theory (DFT) is, in principle, exact, because approximations only take place when we have to choose the form of the exchange-correlation energy functional $E_{xc}[\rho]$ and the corresponding potential V_{xc} . Since the electronic density of the ground state is not known, the Kohn-Sham equations must be solved self consistently, as shown schematically in Fig. 2.1 below.

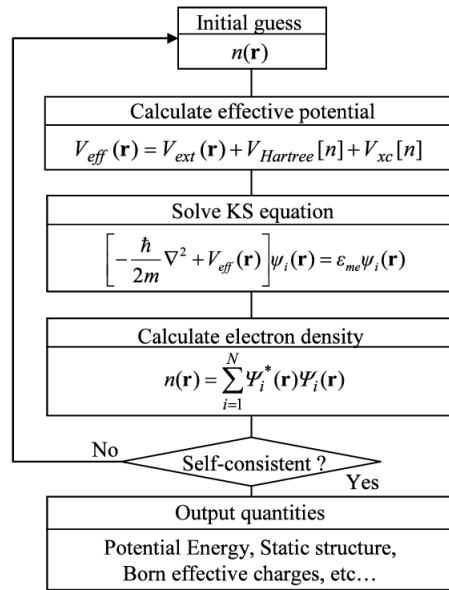


Fig. 2.1: Representation of the self-consistent loop for solution of Kohn-Sham equation [62].

2.4.3 Exchange and Correlation Functional

One of the major issues of Density Functional Theory is to find the most suitable exchange-correlation functional for the studied systems. However, the exact form of these functionals is unknown, thus hampering the way to the exact description of the electronic problem. The accuracy of a numerical calculation based on DFT is, then, checked by comparison with reference data, like those from experiments. Citing some of the widely used functionals in DFT-based calculations, we have LDA (Local Density Approximation) [61] and GGA (Generalized Gradient Approximation) [63]. They are discussed in the following subsections as representative examples.

LDA (Local Density Approximation)

This approximation uses the idea of a homogeneous electron gas for density mapping [61]. It was proposed by Kohn and Sham in the original paper of 1965 where they announced their approach to DFT. In this model, it is considered that the solids in the $N \Rightarrow \infty$, and $V \Rightarrow \infty$ limit, with $\frac{N}{V} = \rho$, are similar to a homogeneous electron gas. Despite its simplicity, this approach yields very good results for some systems, providing results close to those provided by the Hartree-Fock method, which presents a higher computational cost [64]. We can write the LDA functional as follows

$$E_{XC}^{LDA}[\rho] = \int \rho(r) \varepsilon_{xc}(\rho(r)) dr. \quad (2.33)$$

where $\varepsilon_{xc}(\rho(r))$ is the exchange-correlation energy per particle of a uniform electron gas with density $\rho(r)$. It can be rewritten as

$$\varepsilon_{xc}(\rho(r)) = \varepsilon_x(\rho(r)) + \varepsilon_c(\rho(r)), \quad (2.34)$$

with the exchange energy $\varepsilon_x(\rho(r))$ being exactly known [60]. However, the same does not happen to the correlation energy $\varepsilon_c(\rho(r))$, which is obtained approximately.

In general, LDA provides better results for homogeneous systems than for non-homogeneous systems [60]. From the LDA, many other approaches to E_{xc} the functional were developed. One of them is the GGA (Generalized Gradient Approximation), which is a more complex approach to the functional since it involves not only the density but also its gradient. The GGA is, in principle, more suitable for systems where the density ($\rho(r)$) varies rapidly. The LDA has a tendency to overestimate bond energies and underestimate bond lengths, while the GGA tends to the opposite. Both approximations underestimate the band gap [65].

GGA (Generalized Gradient Approximation)

In the generalized gradient approximation (GGA) [63], in addition to considering the electronic density, $\rho(r)$, where the exchange-correlation energy is calculated, we also take into account the gradient of this density. Therefore, the exchange-correlation term can be written as

$$E_{XC}^{GGA}[\rho] = \int \varepsilon_{xc}[\rho(r), \nabla\rho(r)] dr. \quad (2.35)$$

The fact that we use not only the density $\rho(r)$ at a given point, but also its gradient $\nabla\rho(r)$, is justified by the necessity to take into account the rapid variation of the electronic density of a system where the density is not uniform. Unlike LDA, there are different parametrizations for the exchange-correlation term $\varepsilon_{xc}[\rho(r), \nabla\rho(r)]$ and these different parametrizations give rise to different functionals, for example, PBE [63], PBEsol [66] and WC [67]. The most used GGA parametrization is the one developed by Perdew, Burke and Ernzerhof [68], which we used in this work.

2.5 Other Approximations in Electronic Structure

2.5.1 Localized Basis Set

In all approaches to solve the electronic problem, one has to choose the algebraic representation for the electronic orbitals [55]. Among different ways to do it, we choose here a very used method to expand the electronic wavefunctions, which is by the use of numerical atomic orbitals [69]. This approach comes from the idea that the orbitals are mostly localized at the atomic sites and the wavefunctions goes to zero at large distances. Therefore, performing molecular calculations using atomic orbitals centered at the atoms as a basis set is known as Linear Combination of Atomic Orbitals (LCAO).

2.5.2 Mesh-Cutoff

In order to solve the Kohn-Sham Hamiltonian, (Eq. 2.31), some terms of the potential have to be calculated in the real-space [69]. The real-space grid defined to perform such calculations is given by the mesh-cutoff parameter. It represents the highest energy of the plane waves that

can be represented in the grid [69]. It is important to stress that the grid cutoff defined in the LCAO context is not directly comparable to the energy cutoff in the context of plane waves codes [69]. The relationship between the energy cut E_{cut} and the grid interval Δx is given as follows

$$E_{cut} = \frac{\hbar^2 k^2}{2m}, \quad (2.36)$$

with $k = \frac{\pi}{\Delta x}$, which in atomic units becomes

$$E_{cut} = \frac{1}{2} \left(\frac{\pi}{\Delta x} \right)^2. \quad (2.37)$$

From Eq. 2.37, we can state that a higher value of the mesh-cutoff yields a finer real-space grid and, therefore, more accurate results. The way this grid is defined will have strong influence on how accurate the results will be.

2.5.3 Pseudopotential

Another approximation for DFT-based calculations is the pseudopotential theory [70], where the charge density is divided into core and valence contributions. The core is defined as the nucleus plus the core electrons (non-valence) together. The use of pseudopotentials is based on the fact that the electrons, close to the nucleus, participate poorly in chemical bonds and are, therefore, taken to be part of the inner core together with the nucleus. Thus, the pseudopotential is an effective potential felt by the valence electrons and generated by the nucleus and the core electrons. It replaces the real potential felt by the valence electrons. Therefore, only the valence electrons are considered explicitly in the electronic structure calculation. This reduces the computational cost substantially. The pseudopotentials must obey the following properties in order to be considered norm-conserving [70]:

- a) Real and pseudo eigenvalues must be the same for the same atomic configuration;
- b) The real and pseudo wavefunctions must be equal beyond a chosen “core radius”, $r > r_c$;
- c) The integral of the real and pseudo charge density must agree when integrated up to r_c for each valence state;
- d) The logarithmic derivatives of the real and pseudo wavefunctions and their first energy derivatives must be equal for $r > r_c$.

The properties c) and d) are indispensable for the pseudopotential to have an optimum transferability among a variety of chemical environments in self-consistent calculations in which the pseudo charge density is treated as a real physical quantity [70].

Among the different approaches, the Troullier-Martins pseudopotential is one of the most used models, due to the fact that it produces smooth potentials. Moreover, the pseudofunctions have no nodes in the core region, what makes the integrals calculations in the real-space grid much faster. As a result, the total energy of the system and its physical properties present a fast convergence with the improvement of the basis set [71].

By the concepts discussed above, it is restated that DFT is an exact theory that predicts the properties of all states of a system. However, we are limited, in practice, by different factors, such as the exchange-correlation functional. Pseudopotentials are an additional approximative tool to minimize the computational cost. Regarding excited states, even though the DFT, in principle, allows their determination, it has not been possible to develop practical methods for this purpose yet, which has disseminated the wrong idea that DFT is only a ground state theory.

2.6 Computational Details

2.6.1 SIESTA

In order to implement the DFT formalism and perform the electronic structure calculations contained in this work, the SIESTA¹ package was used. SIESTA performs self-consistent calculations using the previously described DFT theory and it is based on the linear combination of atomic orbital (LCAO) approach for the basis set [69] in the expansion of the electronic wavefunctions. In the following, we show the Kohn-Sham Hamiltonian and the basis set for the expansion of the electronic states used in SIESTA. The standard KS one-electron Hamiltonian may be written as [69]

$$\hat{H} = \hat{T} + \sum_I V_I^{local}(\mathbf{r}) + \sum_I \hat{V}_I^{KB}(\mathbf{r}) + V_H(\mathbf{r}) + V_{xc}(\mathbf{r}), \quad (2.38)$$

where I is an atom index, \hat{T} is the kinetic energy operator, $V_I^{local}(\mathbf{r})$ and $\hat{V}_I^{KB}(\mathbf{r})$ are the local and nonlocal (Kleinman-Bylander) [72] parts of the pseudopotentials, $V_H(\mathbf{r})$ and $V_{xc}(\mathbf{r})$ are the total Hartree and the exchange-correlation potential of atom I .

The local part of the pseudopotential is a long-range operator. In order to eliminate the long range in \mathbf{r} , it is defined a basis set for the expansion of the electronic states. It will consist of pseudo valence orbitals of limited range. Therefore, the Kohn-Sham Hamiltonian problem is cast mathematically into the LCAO method.

¹Spanish Initiative for Electronic Simulation with Thousands of Atoms

Regarding the basis functions, if we use one basis function for each valence orbital, we have the so called *single-zeta* (SZ) basis. Using two basis functions for each orbital, we have, then, a *double-zeta* basis (DZ). Aiming to provide an even more complete basis, polarization orbitals can be included, i.e., *double-zeta* plus polarization (DZP).

In summary, we performed the electronic structure calculations using DFT theory by means of SIESTA code [69]. The GGA functional is chosen to represent exchange-correlation energy and a DZP basis set is used to expand the electronic wavefunctions. A 400 Ry mesh-cutoff was used for the real-space integrations. A total of 46 (30) Monkhorst-Pack k-points were used for the BZ integration for the shortest (longest) 1D system not only for the convergence, but also for the calculation of all the physical quantities we investigated.

Chapter 3

Results

In this chapter we present and discuss our electronic structure study on proposed 1D and 2D systems having a naphthyl unit as basic building block. We demonstrate that these materials show distinct physical properties in comparison to graphene.

3.1 Two Dimensional Systems

The systems proposed in this work, which we named *naphthylenes*, are formed by different arrangements of naphthyl units into a 2D lattice. These structures are composed by the same basic building block, but they differ regarding their assembling. The unit cell of the so called naphthylene- α contains 30 atoms, while the structure we named naphthylene- β has 10 atoms in the unit cell. An illustration of their atomic structure is shown in Fig. 3.1 a) and d). The basic unit blocks (naphthyl groups) are joined to each other by square rings in both cases. On one hand, the α case shows 12 and 9-membered rings while in the other hand, the β structure features 10-membered rings as resulting from the particular assembling of its elementary parts. It is important to stress that the BZ for naphthylene- α is similar to that of graphene, namely a regular hexagon. This is because its lattice vectors ($|\vec{a}_1| = |\vec{a}_2| = 10.33 \text{ \AA}$) form an angle of 60° between them. However, while still being hexagonal, the BZ for naphthylene- β is not a regular polygon, since the angle between the lattice vectors ($|\vec{a}_1| = |\vec{a}_2| = 5.61 \text{ \AA}$) is about 73.5° .

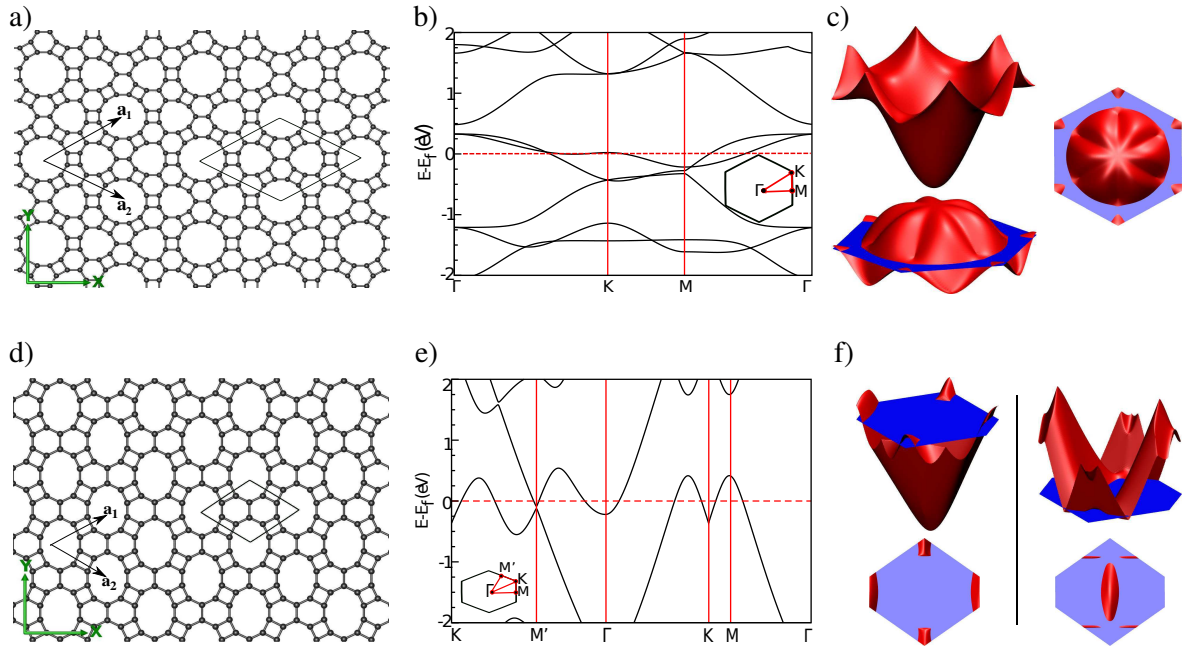


Fig. 3.1: a) Naphthylene- α atomic structure together with its unit cell, b) Electronic band structure of naphthylene- α plotted along high-symmetry direction on the BZ, c) Plot of the valence and conduction bands over the entire BZ. The same information for naphthylene- β is displayed in d), e) and f), respectively.

Concerning the C-C bond lengths, naphthylene- α and naphthylene- β are different from graphene whereby all the C-C bonds have the same length (about 1.42 Å). In Fig. 3.2 we show the different C-C bond lengths for each two-dimensional system considered here.

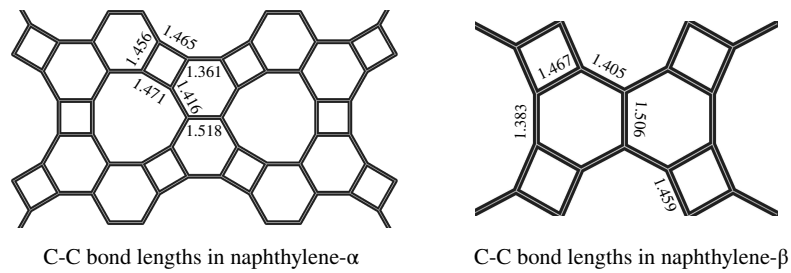


Fig. 3.2: C-C bond lengths (in Å) in naphthylene- α and naphthylene- β , respectively.

Note that the bond lengths vary in the 1.361 Å-1.518 Å range for the α case, while the C-C distance runs from 1.383 Å to 1.506 Å in the β sheet. These different C-C bond lengths strongly suggest a non-delocalized character of the electronic states in the structure, what is quite different from most of sp^2 carbon systems described so far [24]. Usually, in sp^2 carbon

structures, such as graphene, there are no distinct single or double bonds once the electrons of C-C bonds are distributed equally among each C atom [24]. As a consequence, all the bonds have the same length. Figure 3.1 also shows the electronic band structures (b, e) along high-symmetry lines of their Brillouin zones, and a plot of the valence and the conduction bands over the entire BZ (e, f) for both naphthylene systems. They present a metallic behavior once the electronic bands cross the Fermi level, which is located at 0 eV. Naphthylene- α electronic band structure displays some localized states at the Fermi level along the Γ - K line, while for naphthylene- β we see that the bands cross the Fermi level.

It is well known that sp^2 carbon nanostructures with ribbon like geometry can have electronic properties dramatically different from their 2D counterparts [1, 15]. Therefore, after obtaining the electronic band structure of the 2D carbon nanostructures previously presented, we propose to study the nanoribbons that can be constructed from naphthylene- α and naphthylene- β sheets.

3.2 Naphthylene- α Nanoribbons

In this section we present and discuss the electronic properties of nanoribbons conceptually formed from naphthylene- α sheet. We focus on data related to electronic band structures, local density of states and projected density of states.

3.2.1 Studied Structures

For naphthylene- α based nanoribbons, we “cut” and analyzed distinct nanoribbons considering different periodic directions and edges. These two first families of nanoribbons we considered are displayed in Fig. 3.3 and are periodic in the Y direction of naphthylene- α (corresponding to the direction of the \vec{a}_1 - \vec{a}_2 lattice vector). Figure 3.3 a), b) and c) show zigzag naphthylene nanoribbons (ZNNRs) with different widths (w) and the same type of edge (hsh). This nomenclature was chosen because the edge atoms are part of two hexagons connected by a square (hsh) and the bonds on this edge resemble the zigzag type (Z). The width (w) of these NNRs is defined by the number of dodecagon lines parallel to the periodic direction. On the other hand, in Fig. 3.3 d), e) and f) , we have ZNNRs with different widths (w), also determined by the number of dodecagon lines parallel to the periodic direction, and with another type of edge (hh), where hh means that the edge atoms are part of two hexagons.

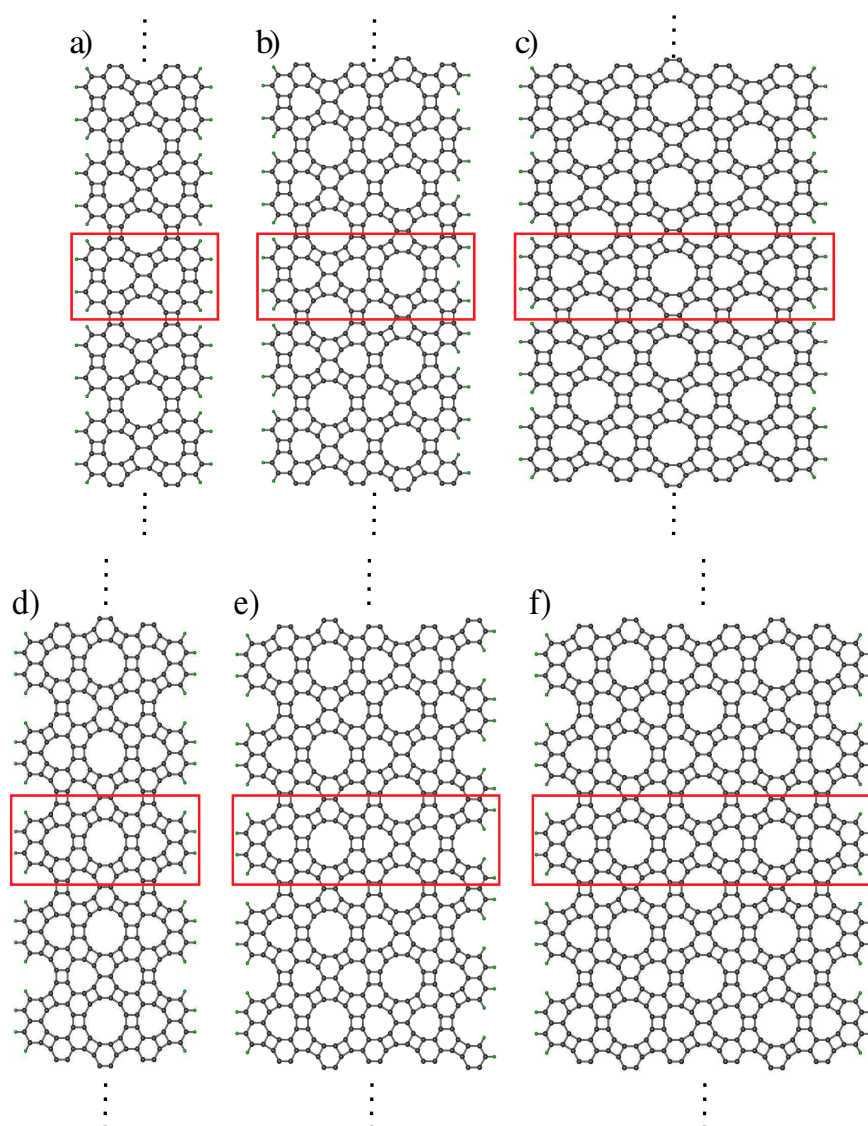


Fig. 3.3: a) α ZNNR-hsh ($w = 1$), b) α ZNNR-hsh ($w = 2$), c) α ZNNR-hsh ($w = 3$), d) α ZNNR-hh ($w = 1$), e) α ZNNR-hh ($w = 2$), f) α ZNNR-hh ($w = 3$) nanoribbons. The box in red highlights the unit cell of the nanoribbons.

For the X direction as the periodic orientation (corresponding to the direction of the $\vec{a}_1 + \vec{a}_2$ lattice vector), we have ANNRS with two types of edges (hh and h), where the ANNRS term is due to the fact that the edge bonds are similar to the armchair type edge (A) in conventional graphene nanoribbons [42]. The hh means that the most peripheral atoms in the non-periodic direction form two hexagons and h means that we have an edge formed by single units of hexagons. Figure 3.4 a), b), and c) represent different widths for the h edge and Fig. 3.4 d), e) and f) display different widths for the hh edge type. In a similar way, the width of the NNRs are also determined by the number of dodecagon lines parallel to the periodic direction.

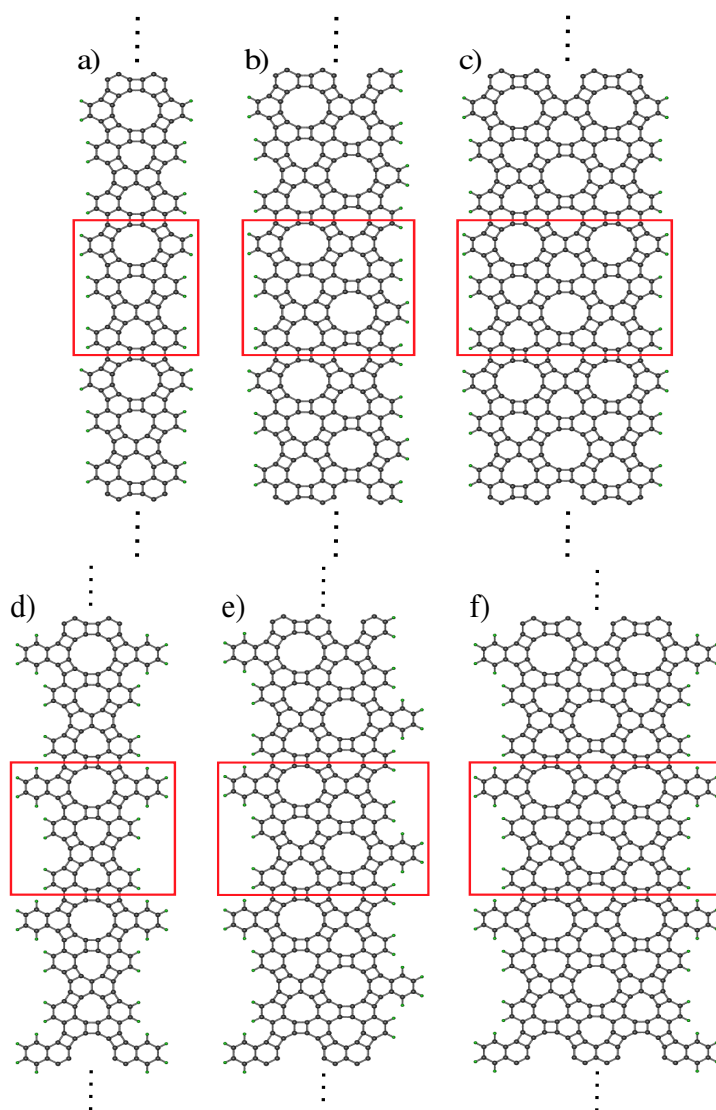


Fig. 3.4: a) α ANNR-h ($w = 1$), b) α ANNR-h ($w = 2$), c) α ANNR-h ($w = 3$), d) α ANNR-hh ($w = 1$), e) α ANNR-hh ($w = 2$), f) α ANNR-hh ($w = 3$) nanoribbons. The box in red highlights the unit cell of the nanoribbons.

For each family of NNRs, there is a simple equation that relates the number of carbon atoms by unit cell with the width w of the ribbon, as shown in Table 3.1.

Tab. 3.1: Number of carbon atoms by unit cell as a function of the width of the ribbon.

Family of Ribbons	Number of Carbon Atoms
α ZNNR-hsh	$30w+20$
α ZNNR-hh	$30w+40$
α ANNR-h	$30w+32$
α ANNR-hh	$30w+40$

The number of hydrogen atoms in a unit cell is 16, 12, 8, and 8 in α ANNR-hh, α ANNR-h, α ZNNR-hh, and α ZNNR-hsh systems, respectively.

3.2.2 Electronic Band Structures and Local Density of States

In this section, we present the electronic properties of the 1D systems obtained from naphthylene- α . We show band structures and a plot of their Local Density of States (LDOS) around the Fermi level (integrated from -0.1 eV to 0.1 eV) in order to verify how these states are arranged in the structures. In these calculations, we do not consider spin polarization. Figure 3.5 also shows the LDOS plot for the α ZNNR-hsh nanoribbons along with their electronic band structures.

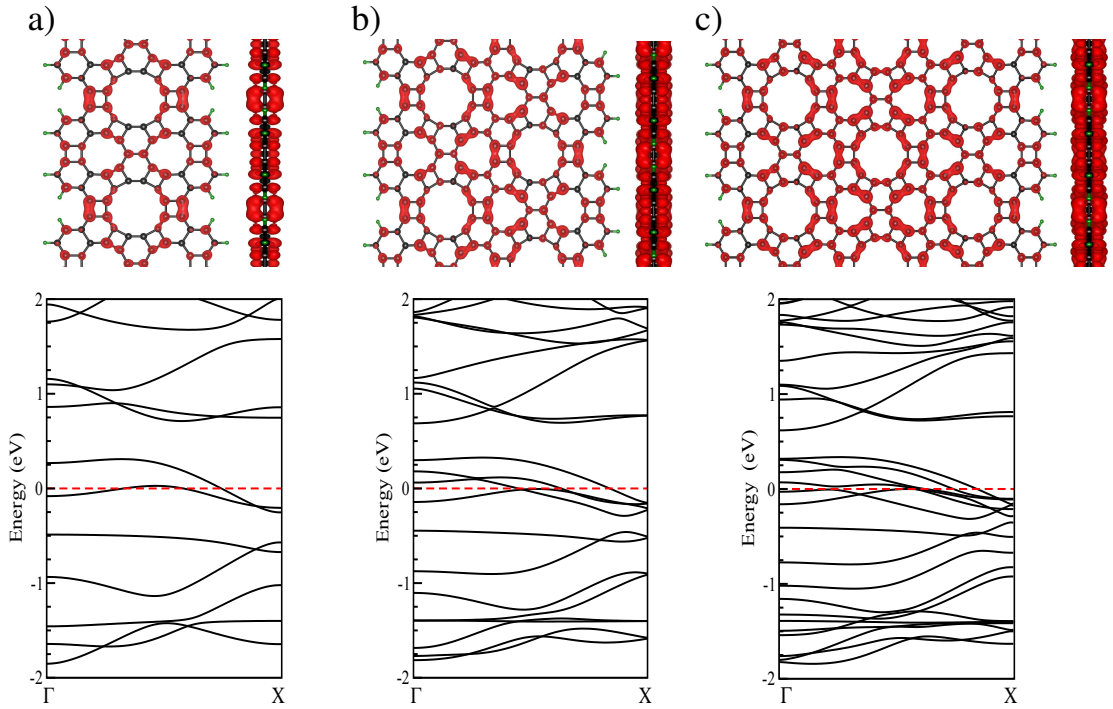


Fig. 3.5: LDOS plot (front and side view) for α ZNNR-hsh a) $w = 1$, b) $w = 2$ and c) $w = 3$ nanoribbons from -0.1 eV to 0.1 eV around the Fermi level along with their electronic band structures. Isosurface value of 0.002.

The three studied ribbons from the α ZNNR-hsh family present a metallic behavior. In addition, we see that the number of levels crossing the Fermi level increases for wider ribbons. Therefore, since the edges do not change with the increasing of the width, it suggests that these states are not edge states (as we have in traditional graphene nanoribbons [41, 42, 73]), but rather inner states. This is verified from the LDOS plot. In special for $w = 3$, note that these frontier states are mainly concentrated in the middle of the ribbon. Besides that, these states are not equally distributed among the atoms, what was already suggested by the different bond lengths in the structure. Most of them are localized in the bonds between two naphthyl units.

The side view plot of the LDOS is shown to reassure the majority of π orbitals as we already expect for sp^2 carbon materials.

Fig. 3.6 displays the LDOS plot for the α ZNNR-hh a) $w = 1$, b) $w = 2$ and c) $w = 3$ nanoribbons along with their electronic band structures.

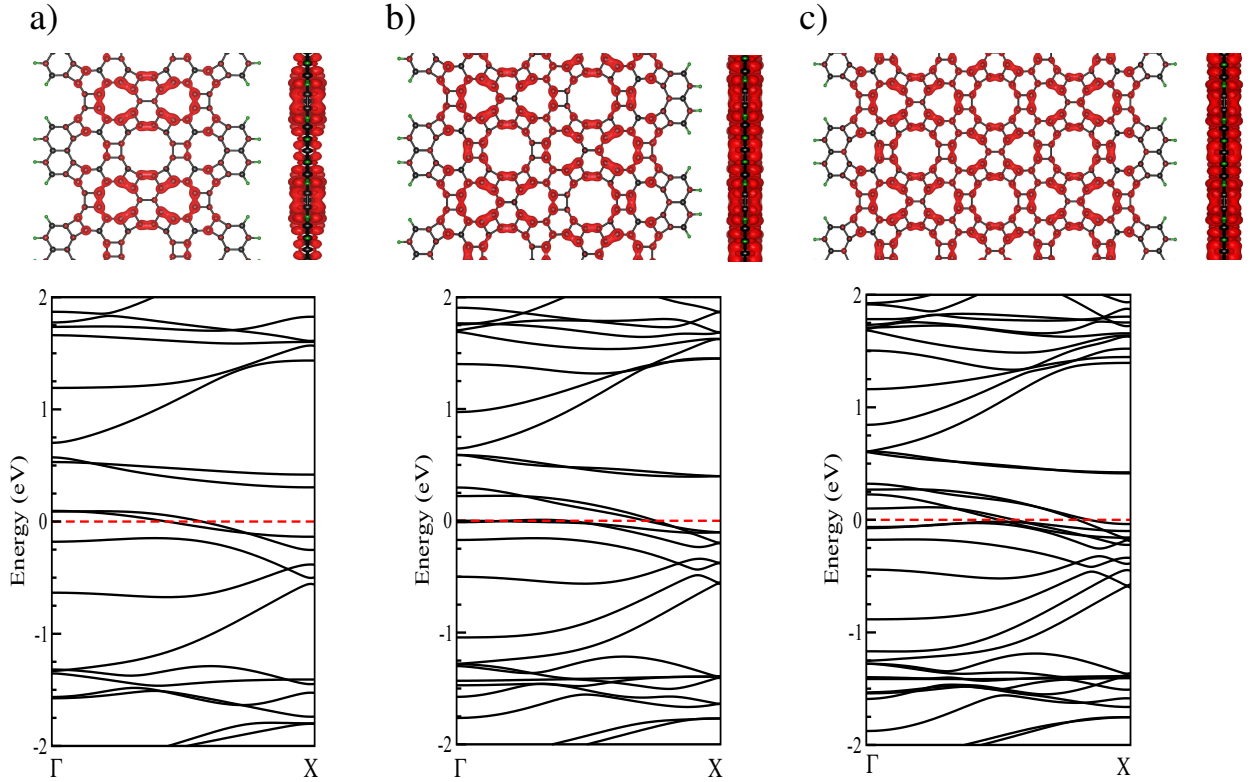


Fig. 3.6: LDOS plot (front and side view) for α ZNNR-hh a) $w = 1$, b) $w = 2$, and c) $w = 3$ nanoribbons from -0.1 eV to 0.1 eV around the Fermi level along with their electronic band structures. Isosurface value of 0.002 .

For this family of ribbons shown in Fig. 3.6, we have that all of them also present a metallic behavior as the family of ribbons previously discussed. Similarly, the states near the Fermi level are not edge states. The LDOS side view plot shown for all these three systems allows us to confirm the predominance of π orbitals around the Fermi level. The similarities between these two families of ZNNRs is a consequence of the inner character of the states around the Fermi level, so that they are only slightly affected by details of the edge structure.

We now move to the armchair families of naphthylene nanoribbons. In Fig. 3.7 we show the LDOS plot and the electronic band structures for the α ANNR-h nanoribbons, which are periodic in the X direction of naphthylene- α sheet.

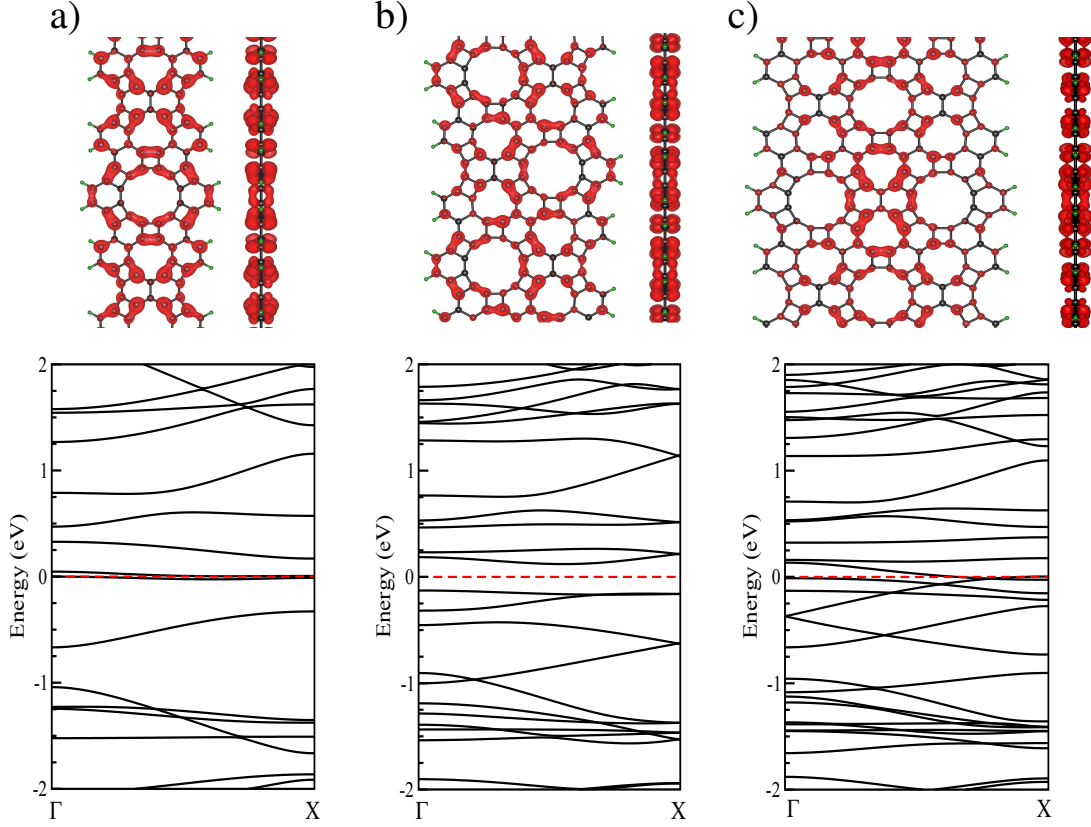


Fig. 3.7: LDOS plot (front and side view) for α ANNR-h a) $w = 1$, b) $w = 2$, and c) $w = 3$ nanoribbons from -0.1 eV to 0.1 eV (except for $(w = 2)$) around the Fermi level along with their electronic band structures. Isosurface value of 0.002 .

Except by a single system, these ribbons also present a metallic behavior. The second structure, α ANNR-h ($w = 2$), displays an indirect band gap of approximately 0.25 eV. Therefore, instead of plotting its LDOS from -0.1 eV to 0.1 eV, we considered the entire region containing some valence and some conduction bands (from -0.17 eV to 0.22 eV) for this particular system. These states are mainly localized at the bonds between the naphthyl units. The electronic band structure for α ANNR-h ($w = 1$) shows flat bands at the Fermi level. In addition, these flat bands also indicate the possibility to obtain spin polarized structures (as in the case of ZGNRs [41]), which will be discussed in a later section. From the electronic band structure of the third structure, α ANNR-h ($w = 3$), we see that this system is also metallic, but with less localized electronic states at the Fermi level in comparison with the first system. From its LDOS plot, we observe that most of the states are localized around the second line of pores of the ribbon.

Similarly to the previous families studied, these are inner states.

Figure 3.8 shows the LDOS plot and the electronic band structures for the α ANNR-hh nanoribbons, which are also periodic in the X direction of naphthylene- α .

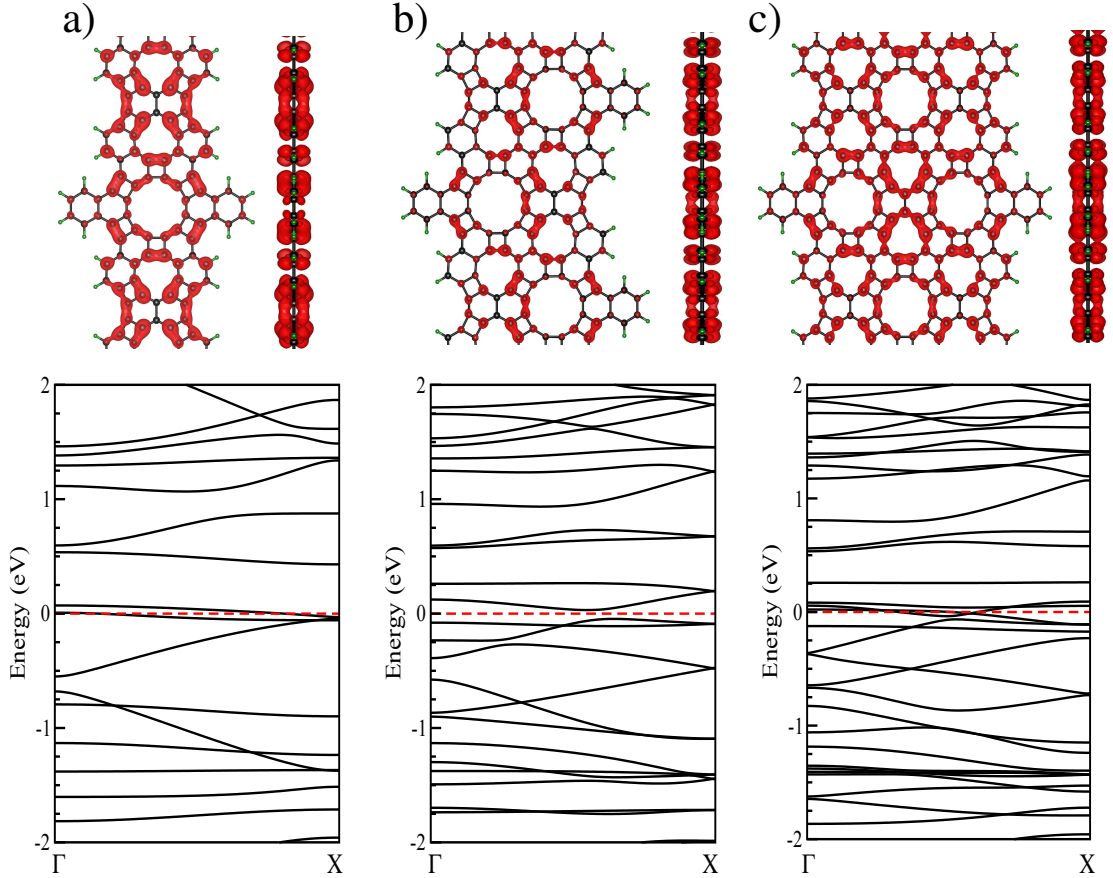


Fig. 3.8: LDOS plot (front and side view) for α ANNR-hh a) ($w = 1$), b) ($w = 2$), and c) ($w = 3$) nanoribbons from -0.1 eV to 0.1 eV around the Fermi level along with their electronic band structures. Isosurface value of 0.002 .

Similarly to the α ANNR-h ($w = 1$), the α ANNR-hh ($w = 1$) system presents flat bands near the Fermi level. The second structure of this family, α ANNR-hh ($w = 2$), displays a very small indirect band gap of approximately 0.08 eV. Regarding the third ribbon, α ANNR-hh ($w = 3$), once again we have an increase in the number of levels around the Fermi level, showing that these states are distributed over the structure and not only localized at the edges, what is also true for the two first systems of this family of nanoribbons. A difference between the armchair and the zigzag ribbons is that the frontier bands are more dispersive in the zigzag configurations. Once again, due to the inner aspect of the frontier states, the ANNRS show to be weakly influenced by details of the edge structure.

It is known that zigzag graphene nanoribbons (ZGNRs) present a magnetic ordering as a consequence of electron spin polarization [15]. We note that some of our studied systems show localized levels at the Fermi energy, which can result in spin polarization, as discussed, for instance, for graphene flakes [74]. Therefore, we proceeded with spin polarized calculations in order to investigate the possible existence of such states in α NNRs. The following section presents and discusses the ribbons that converged to either antiferromagnetic (AFM) or ferromagnetic (FM) states.

3.2.3 Spin Polarization

Considering all the nanoribbons *constructed* from naphthylene- α previously studied, we verified the possibility to obtain ferromagnetically and antiferromagnetically polarized systems. When the spin orientation of neighbor particles are opposite, we say they are antiferromagnetically aligned. On the other hand, when all the moments are aligned in the same direction, they are ferromagnetically aligned. All the systems, except by the α ANNR-h ($w = 1$) and α ANNR-hh ($w = 1$) nanoribbons displayed in Fig. 3.9, converged to the non polarized (NP) state. The flat bands around the Fermi level for these two systems in the NP state already suggested a magnetic ordering. The absence of such magnetic states in the zigzag systems is not surprising, as their bands around the Fermi level are dispersive, as well as it is the case for the frontier bands of wide armchair systems, which become more dispersive for increasing width. As shown for several carbon structures, the existence of localized levels is a fundamental ingredient for the emergence of spin polarized states [15, 41, 42, 74, 75]. Figure 3.9 shows α ANNR-h ($w = 1$) and α ANNR-hh ($w = 1$) nanoribbons along with their electronic band structures in different states.

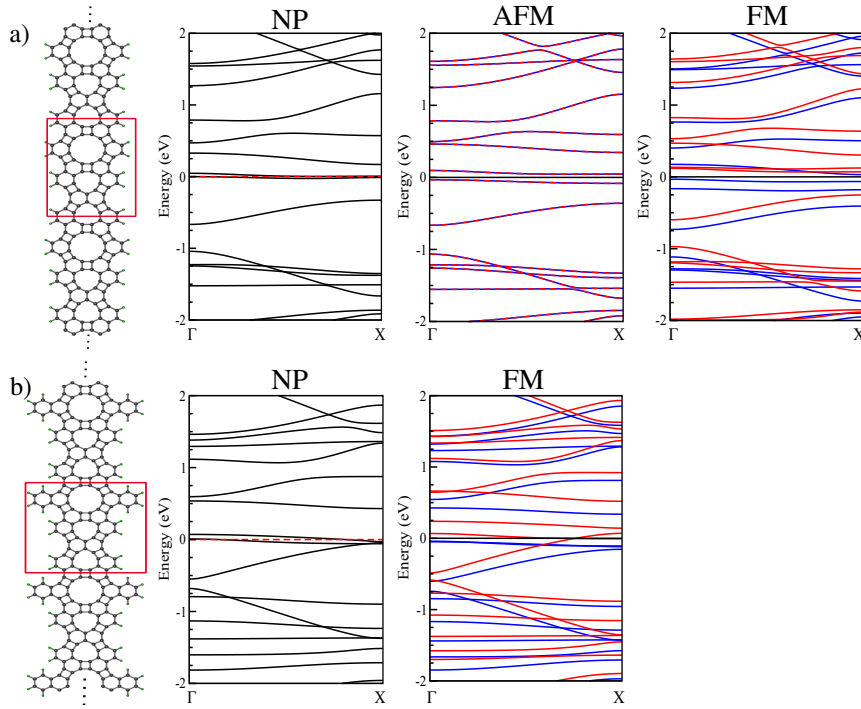


Fig. 3.9: a) α ANNR-h ($w = 1$), b) α ANNR-hh ($w = 1$) nanoribbons along with the electronic band structures for the non polarized (NP), antiferromagnetic (AFM) and ferromagnetic (FM) states, respectively.

Regarding the total energy of the structures, we have that $E_{FM} < E_{AFM} < E_{NP}$ ($\Delta E_{NP-FM} = 0.09$ eV and $\Delta E_{NP-AFM} = 0.05$ eV) for α NNR-h ($w = 1$) and $E_{FM} < E_{NP}$ ($\Delta E_{NP-FM} = 0.05$ eV) for α NNR-hh ($w = 1$). The fact that the FM state is more stable than the AFM state can be explained by the fact that naphthylene- α is not a bipartite lattice as graphene [76].

The most significant change relative to the NP state regarding the electronic band structures of these two ribbons occurs when the systems are in the FM state. The AFM state of the α ANNR-h ($w = 1$) nanoribbon opens a very small band gap (~ 0.08 eV), what also happens in the FM state (~ 0.06 eV). However, in the latter case we clearly see spin up and spin down splitting for the electronic bands, which leads to a magnetic moment of $1.89\mu_B$. The localized states at the Fermi level in the absence of spin polarization are eliminated when the structure is either in AFM or FM state. Regarding the second structure, α ANNR-hh ($w = 1$), we are only able to find a FM state. For the α ANNR-hh, the FM state presents a magnetic moment of $\sim 1.77\mu_B$, which is now slightly lower than the previous case as we now have a set of bands crossing the Fermi level. In this state, the energy levels for spin up and spin down contribution are not degenerated and this structure displays a metallic behavior once the bands cross the Fermi level.

In order to get further insight on these electronic states, we analyze the spin density and density of states (DOS) for the α ANNR-h ($w = 1$) system in the FM state. We divided the structure in two different regions as we show in Fig. 3.10, where we plot the spin polarization for α ANNR-h ($w = 1$) ribbon. The Region 1 is the one involving the dodecagon and the Region 2 involves the two eneagons.

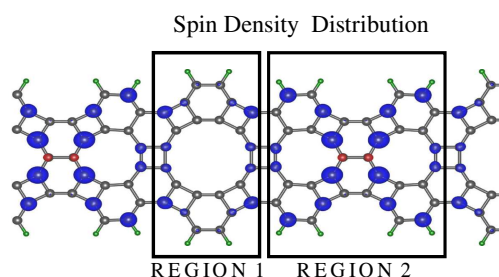


Fig. 3.10: Spin density distribution for the α ANNR-h ($w = 1$) structure.

It is observed from Fig. 3.10 that the spin density is mainly located in the region 2, more precisely around the 4 centered atoms of this region, which belong to the same naphthyl unit.

In addition to the spin distribution, we also investigated the LDOS for the levels near the Fermi level from both spin up and spin down contributions. In Fig. 3.11, we show the band structure and the DOS from spin up contribution for both regions, along with the LDOS plot for the bands from spin up contribution near the Fermi level.

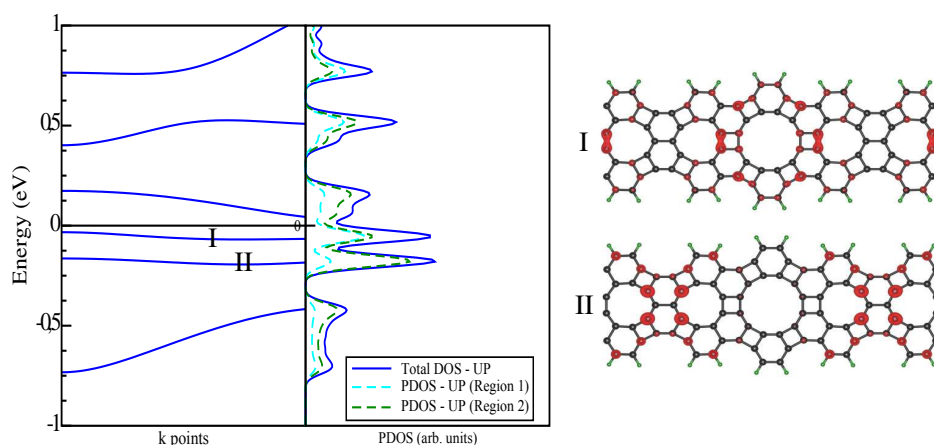


Fig. 3.11: Electronic band structure for spin up states, total DOS (spin up contribution) along with the PDOS (spin up contribution) from REGION 1 and REGION 2, LDOS plot for I and II bands (spin up contribution) around the Fermi level. Isosurface value of 0.0009 for LDOS plot.

We focus our analysis on the first two bands below the Fermi level, which are the main responsible for the systems's magnetic moment. According to Fig. 3.11, we can see from the LDOS plot how these states are distributed over the structure. From the projected density of states (PDOS), we know how each region contributes to the total DOS. We note from the PDOS and LDOS plots that there is a significant contribution to the DOS from the region that contains the two eneagons (Region 2). Note that the state I lies mainly in between regions 1 and 2. On the hand, the state II is predominantly localized in the naphthyl unit between eneagons. In fact, if we take a look at the PDOS information only for the first level below the Fermi level, we have that both regions give almost the same contribution to the DOS. On the other hand, the PDOS for the state II matches the LDOS information on the fact that it is mostly from region 2.

In Fig. 3.12, we show the electronic band structure, the DOS from spin down contribution along with the LDOS plot for the first two spin-down bands above the Fermi level.

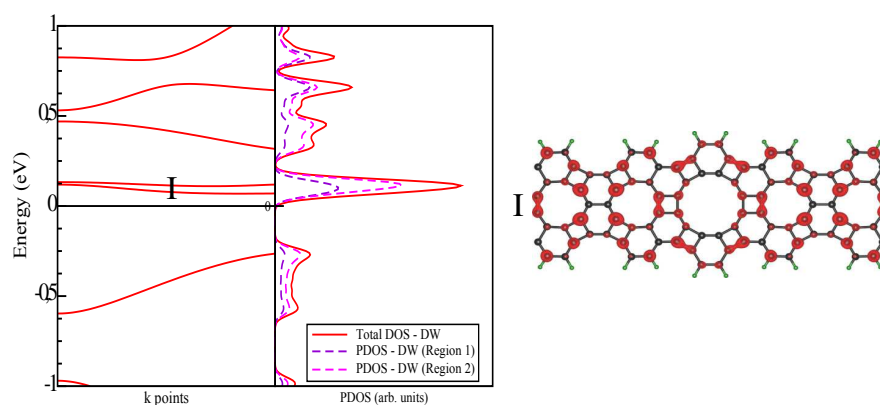


Fig. 3.12: a) Electronic band structure for spin down states, total DOS (spin down contribution) along with the PDOS (spin down contribution) from REGION 1 and REGION 2 and LDOS plot for the two bands (I) (spin down contribution) above the Fermi level. Isosurface value of 0.002 for LDOS plot.

Similarly to the states from spin up contribution, the spin down states are mainly distributed over the region 2 as shown in Fig. 3.12. There is a significant contribution not only from the 4 atoms centered in region 2, but also from the bonds between 2 naphthyl units. In fact, this plot looks like a superposition of the two spin up states below the Fermi energy. These corresponds to the two spin down bands from the unpolarized states which were pushed up by the charge occupying the spin up bands.

3.3 Naphthylene- β Nanoribbons

3.3.1 Studied Structures

Considering the 2D system naphthylene- β , we can also *construct* nanoribbons with different types of edge and periodic directions. The nanoribbons presented in Fig. 3.13 were constructed so that they are periodic in the Y direction of naphthylene- β previously shown. The structures shown in a), b) and c) represent armchair naphthylene nanoribbons (ANNR) with different widths (w) and the same type of edge, hh , since the bonds on the edge resemble the armchair type (A), and the most peripheral atoms on the edge in the non-periodic direction are part of two hexagons. Figures 3.14 a), b) and c) represent three NNRs with the same type of edge (h) and different widths in the same periodic direction, while Figs. 3.14 d), e) and f) show NNRs with different widths, hh edge type and periodic in the X direction. The width (w) of these NNRs were chosen by the number of decagon lines parallel to the periodic direction.

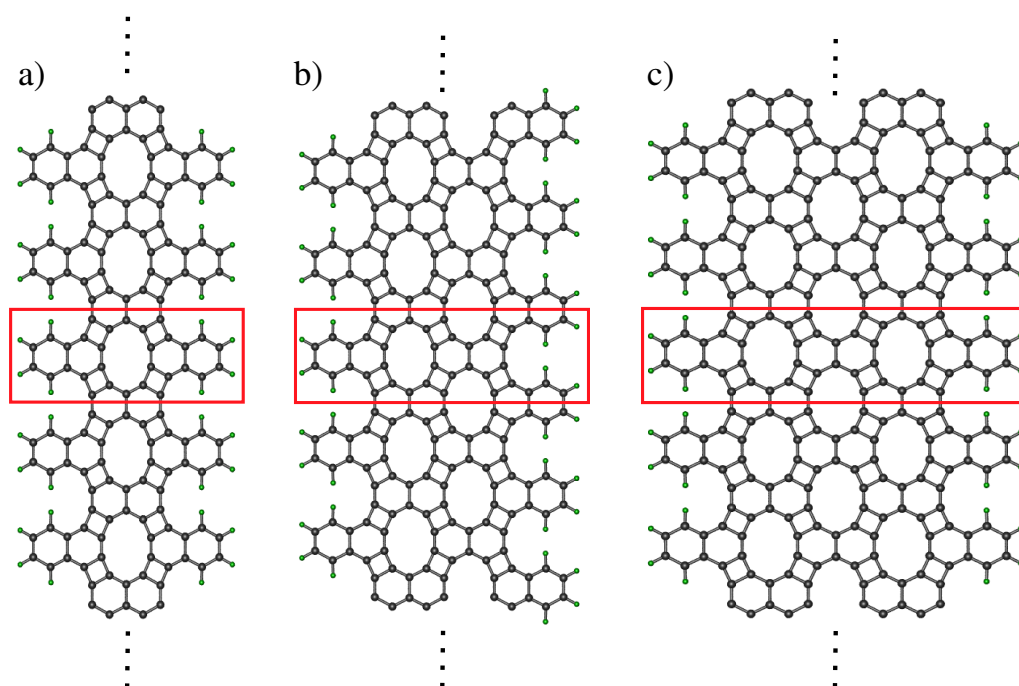


Fig. 3.13: a) β ANNR-hh ($w = 1$), b) β ANNR-hh ($w = 2$), c) β ANNR-hh ($w = 3$) nanoribbons. The box in red highlights the unit cell.

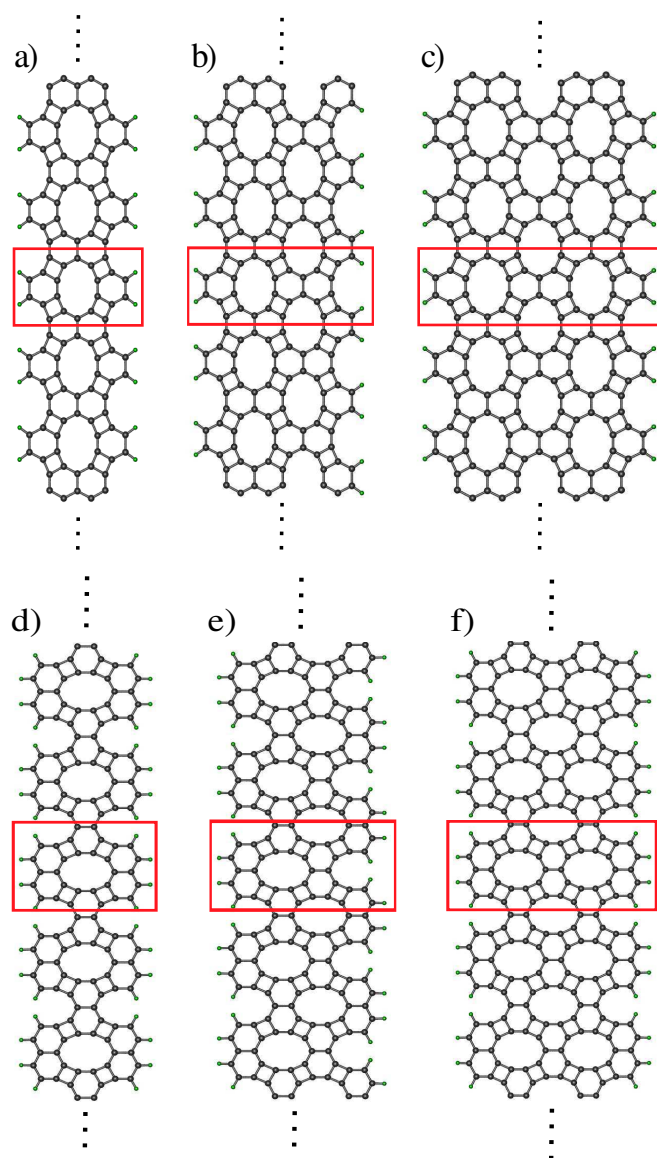


Fig. 3.14: a) β ANNR-h ($w = 1$), b) β ANNR-h ($w = 1$), c) β ANNR-h ($w = 3$), d) β ZNNR-hh ($w = 1$), e) β ZNNR-hh ($w = 2$), f) β ZNNR-hh ($w = 3$) nanoribbons. The box in red highlights the unit cell.

Regarding the number of carbon atoms by unit cell, they are listed in Table 3.2. For each family, there is an equation that relates the number of carbon atoms by unit cell with the width w of the ribbon.

Tab. 3.2: Number of carbon atoms by unit cell as a function of the width of the ribbon.

Family of Ribbons	Number of Carbon Atoms
β ANNRhh	$10w+20$
β ANNRh	$10w+12$
β ZNNRhh	$10w+20$

3.3.2 Electronic Band Structures and Local Density of States

In this section, we present the electronic band structures of the 1D systems obtained from naphthylene- β along with their Local Density of States (LDOS) around the Fermi level (from -0.1 eV to 0.1 eV) to verify how these states are arranged in the structure. Figure 3.15 shows the LDOS plot for the β ANNR-h nanoribbons along with their electronic band structures.

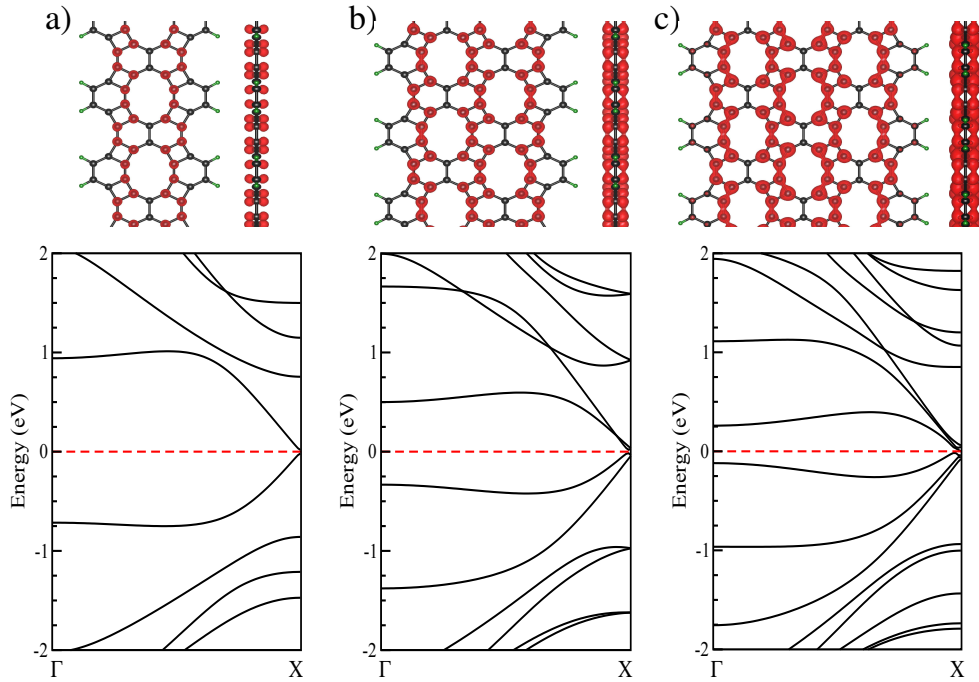


Fig. 3.15: LDOS plot (front and side view) for β ANNR-h a) ($w = 1$), b) ($w = 2$), and c) ($w = 3$) nanoribbons from -0.1 eV to 0.1 eV around the Fermi level along with their electronic band structures. Isosurface value of 0.006.

Unlike naphthylene- α nanoribbons, the states close to the Fermi level lie at the X point of the BZ. In this point, they are in a number which also increases with ribbon width. The conduction and valence bands, get closer to the Fermi level at the Γ point as the ribbons become

larger. The three of them present a metallic behavior and the bands approach each other near the X point of the BZ. Similarly to the previous structures, the density of states is distributed over the whole structure, mainly around the pores, and not only located at the edges as we see in traditional graphene nanoribbons [41]. The side view of the LDOS plot for the three systems shows the majority of π orbitals around the Fermi level.

In Fig. 3.16 we have the LDOS plot and the electronic band structures for the β ANNR-hh nanoribbons.

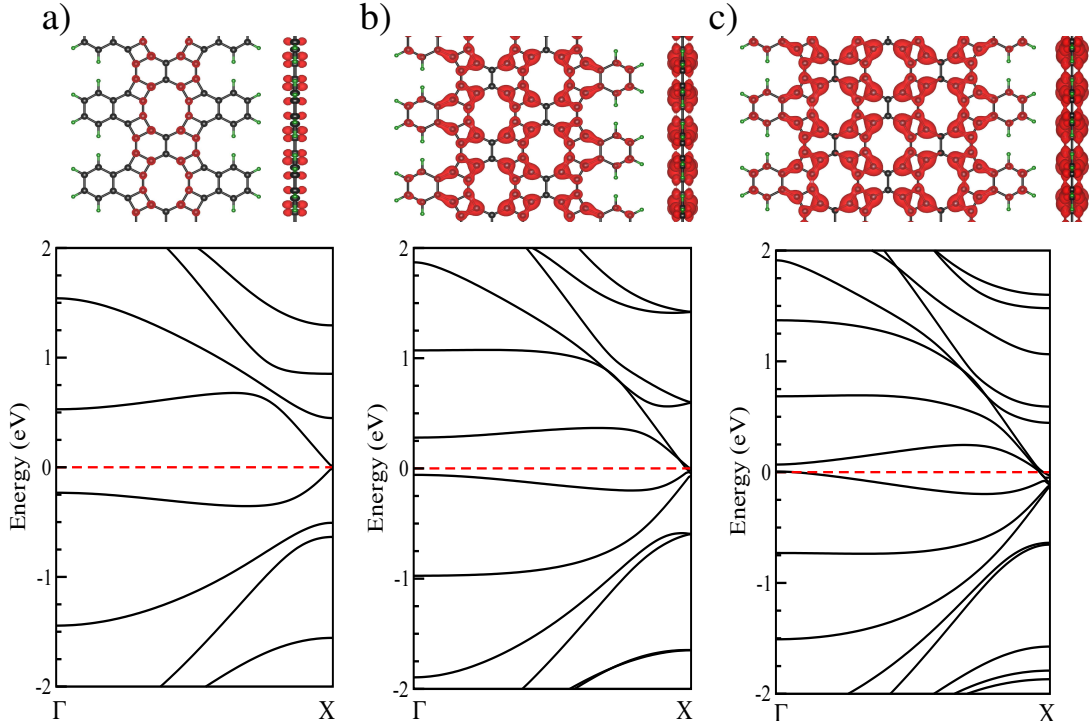


Fig. 3.16: LDOS plot (front and side view) for β ANNR-hh a) ($w = 1$), b) ($w = 2$), and c) ($w = 3$) nanoribbons from -0.1 eV to 0.1 eV around the Fermi level along with their electronic band structures. Isosurface value of 0.0008 .

One can see that these three β ANNR-hh nanoribbons are metallic and, similarly to the β ANNR-h family, the valence and conduction bands meet at the Fermi level at the X point, where they join an additional set of $2(w - 1)$ bands. Therefore, the electronic band structures of β ANNRhh nanoribbons are very similar to those of β ANNR-h once they are different only at the edges and, as we have seen, the edges do not play the most important role in the determination of the electronic properties of the discussed systems in this work. In spite of that similarity, for the β ANNR-hh systems, the conduction and valence bands are closer to the Fermi level at the Γ than those of β ANNR-h nanoribbons with same w .

Figure 3.17 displays the LDOS plot for the β ZNNR-hh nanoribbons, which are periodic in

the X direction of naphthylene- β , along with their electronic band structures.

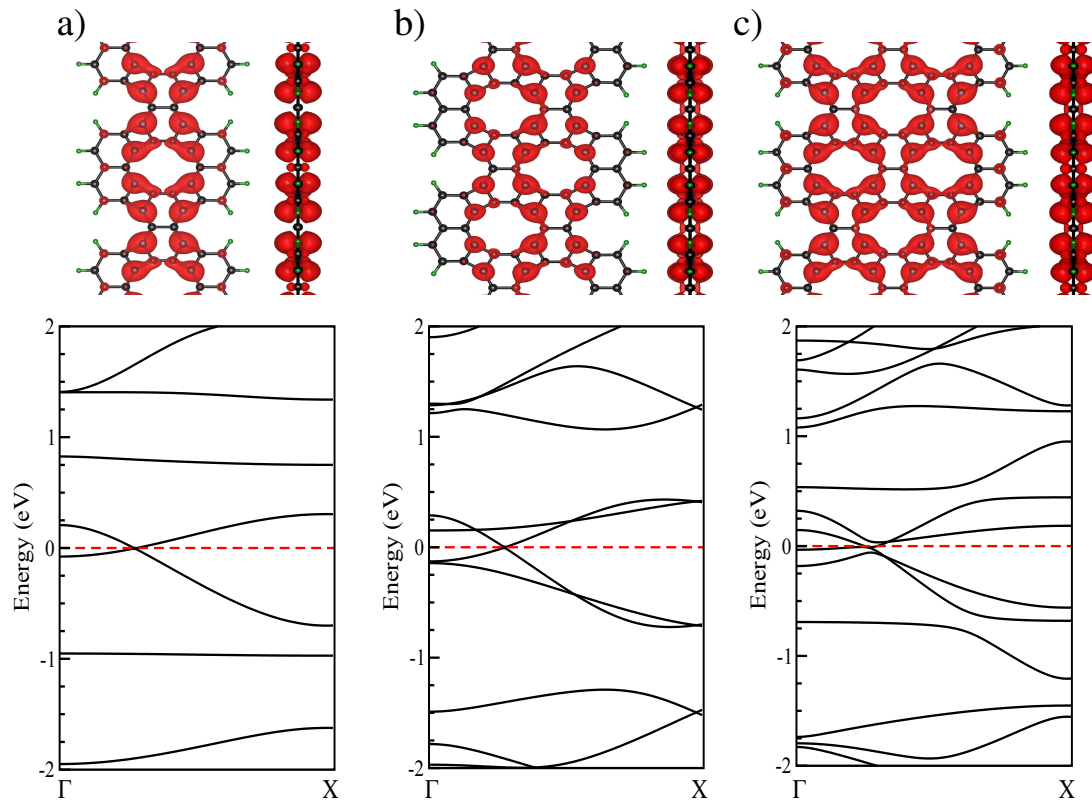


Fig. 3.17: LDOS plot (front and side view) for β ZNNR-hh a) ($w = 1$), b) ($w = 2$), and c) ($w = 3$) nanoribbons from -0.1 eV to 0.1 eV around the Fermi level along with their electronic band structures. Isosurface value of 0.0008 .

From the electronic band structures of the β ZNNR-hh nanoribbons, we can see that the three of them also present a metallic behavior and the valence and conduction bands cross each other between the Γ and X points, almost at the same k point. Regarding the LDOS information, for all the three of them, most of the states are located around the pores of the structures.

3.3.3 Spin Polarization

Considering all the nanoribbons previously presented that were *constructed* from naphthylene- β , we verified the possibility to obtain ferromagnetically and antiferromagnetically polarized systems, but all of them, except those displayed in Fig. 3.18 and Fig. 3.19, converged to the NP state. Figure 3.18 shows the β ANNR-hh ribbons in the NP and AFM states.

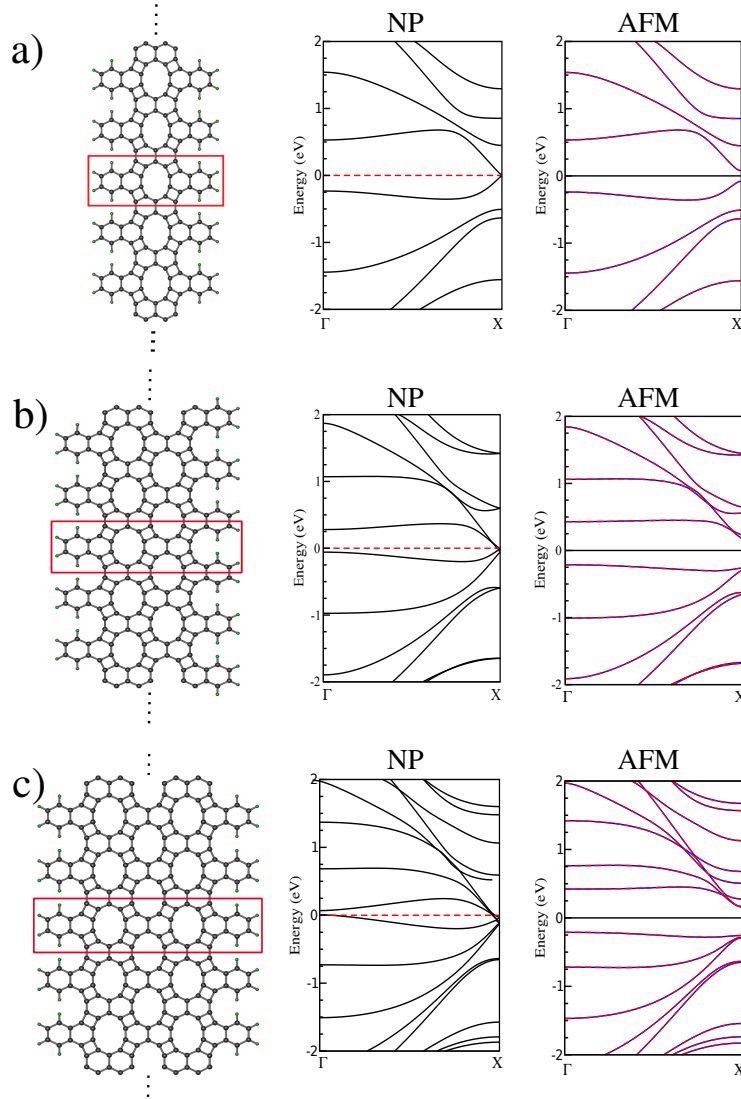


Fig. 3.18: a) β ANNR-hh ($w = 1$), b) β ANNR-hh ($w = 2$), and c) β ANNR-hh ($w = 3$) nanoribbons along with the electronic band structures for the non polarized (NP) and antiferromagnetic (AFM) states, respectively.

From Fig. 3.18a, we can see a ~ 0.14 eV gap for the β ANNR-hh ($w = 1$) ribbon in the AFM state, while in Figs. 3.18b-c, we have a gap opening of ~ 0.40 eV in the AFM state for both

β ANNR-hh ($w = 2$) and β ANNR-hh ($w = 3$). A FM state was not found for these systems. Regarding the total energy, we have that $\Delta E_{NP-AFM} = 0.004$ eV ($w = 1$), $\Delta E_{NP-AFM} = 0.069$ eV ($w = 2$) and $\Delta E_{NP-AFM} = 0.152$ eV ($w = 3$). Figure 3.19 shows the β ZNNR-hh ribbons in different states.

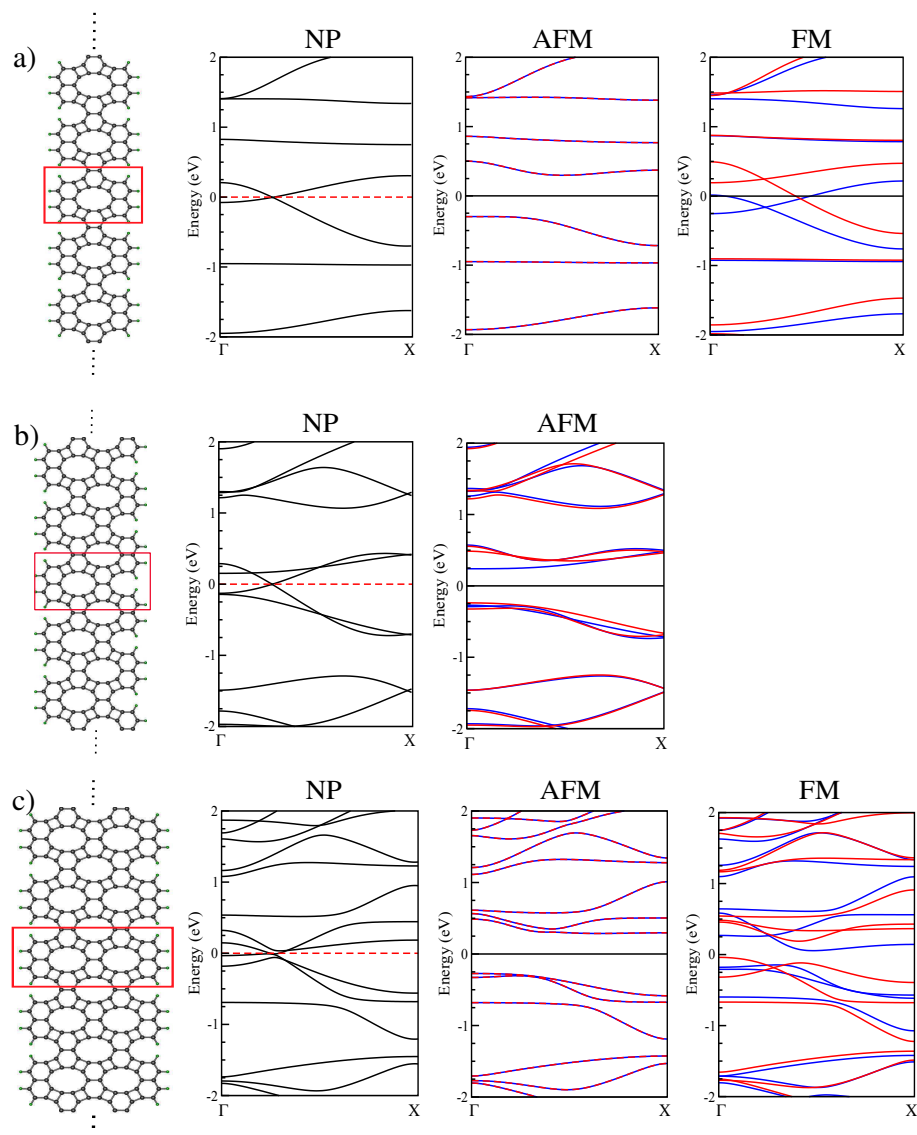


Fig. 3.19: a) β ZNNR-hh ($w = 1$), b) β ZNNR-hh ($w = 2$) and c) β ZNNR-hh ($w = 3$) nanoribbons along with the electronic band structures for the paramagnetic (PM), antiferromagnetic (AFM) and ferromagnetic (FM) states, respectively.

From Fig. 3.19, we can see that the β ZNNR-hh ($w = 1$) and β ZNNR-hh ($w = 3$) structures opened an indirect band gap of approximately 0.60 eV and 0.56 eV, respectively, when in the AFM state, while the $w = 2$ ribbon shows a direct band gap (from a spin-down to a spin-up

level) of 0.47 eV at Γ . In the FM state, β ZNNR-hh ($w = 1$) still presents a metallic behavior as in the NP state, however, the bands from the spin up and spin down contribution have different energy values. Finally, the $w = 3$ ribbon shows an indirect band gap of 0.09 eV. It is important to stress that the $w = 2$ system features only an AFM state, and differently from the other two systems, these bands are not degenerated relative to the spin. This is related to details of the atomic structure, as we discuss below. Concerning the total energy of these systems, we have that $\Delta E_{NP-AFM} = 0.116$ eV and $\Delta E_{NP-FM} = 0.026$ eV for the $w = 1$ system, $\Delta E_{NP-AFM} = 0.139$ eV for $w = 2$, and $\Delta E_{NP-AFM} = 0.212$ eV and $\Delta E_{NP-FM} = 0.09$ eV for the $w = 3$ ribbon.

Aiming to investigate the spin polarized states of these systems proposed from naphthylene- β , we plotted the spin density as shown in the following. Figure 3.20 presents the spin density plot for the β ANNR-hh ribbons in the AFM state.

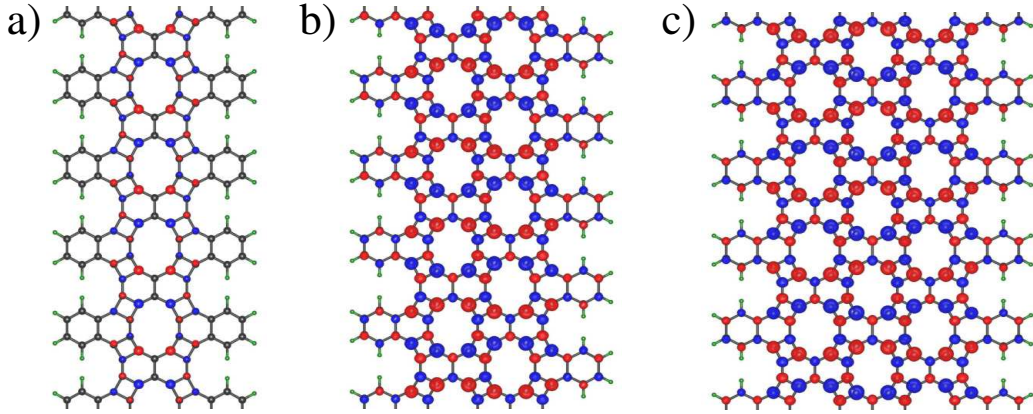


Fig. 3.20: Spin density distribution of a) β ANNR-hh ($w = 1$), b) β ANNR-hh ($w = 2$) and c) β ANNR-hh ($w = 3$) nanoribbons in the AFM state.

Differently from the α case, naphthylene- β features a bipartite network, in the sense that we can split the atoms into two sets, A, and B, so that each atom from A has only neighbors from the set B, and vice-versa. The spin plot from Fig. 3.20 resembles such features, since each atom with spin-up polarization (in blue) is bonded to three atoms with spin-down (in red). Moreover, these 3 ribbons are more stable in the AFM state.

Moving to the β ZNNR-hh systems, in Fig. 3.21 we have a plot of the spin density distribution.

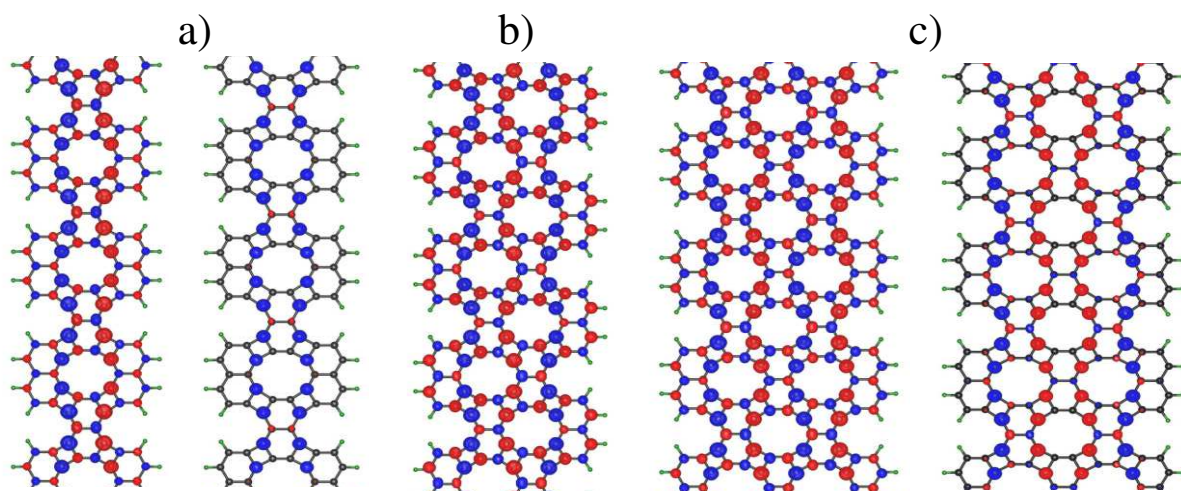


Fig. 3.21: Spin density distribution of a) β ZNNR-hh ($w = 1$), b) β ZNNR-hh ($w = 2$) and c) β ZNNR-hh ($w = 3$) nanoribbons in the AFM and FM state.

The $w = 1$ and $w = 3$ systems converged to both AFM and FM states, differently from the $w = 2$ ribbon that showed only the AFM state. Note that, even with naphthylene- β being a bipartite network, the outmost carbon atoms from opposite edges of the $w = 2$ system belong to the same sublattice, so there is a natural imbalance between the spin resolved electronic clouds, and these atoms present the same spin polarization. This explains why the bands in the AFM state of $w = 2$ are not spin degenerated. Once again, all the β ZNNR-hh systems are more stable in the AFM state.

Chapter 4

Conclusions and Perspectives

In summary, we proposed in this work a class of structures based on naphthyl units, and we studied their electronic properties by means of DFT calculations. These naphthyl units can be arranged in different assemblings, resulting in membranes with distinct kinds of pores, what is an interesting result concerning the potential applications as in gases separation, for example. The two two-dimensional systems originated from the different arrangements of naphthyl groups were named naphthylene- α and naphthylene- β . Besides proposing and investigating the two dimensional systems, it was also constructed and studied different nanoribbon families. From our findings, we can state that these 2D-systems show a metallic behavior, and most of the naphthylene- α , and - β nanoribbons share the metallic character of their 2D counterparts. However, the frontier states in these systems lie in the inner part of ribbon, rather than at their edges, like in zigzag edged graphene nanoribbons. As a result, their electronic properties are mostly determined by chirality, rather than by the details of their edge structure. This property has practical implications for nanotechnological applications, as samples at this size scale commonly contain defects, specially at their edges. This feature can also play an important role on electronic transport properties once inserted into prototypes of nanodevices, since they can provide a more efficient electron injector in nanojunctions having these ribbons as leads. Regarding the spin polarization, few systems converged to spin polarized states.

As perspective, besides investigating other physical quantities for our systems and studying more types of nanoribbons, we also intend to construct and to study naphthylene nanotubes as Koch *et al* proposed to do with graphenylene [50]. In their work, besides investigating the electronic properties of distinct graphenylene nanotubes, they also considered the case of lithium adsorption and showed that graphenylene nanotubes offer a very unique and promising structure for lithium storage [50]. Besides that, we also aim to study naphthylene based systems under effects of hydrogenation/halogenation as performed on graphenylene by Liu *et al* [77].

Liu *et al* studied how the electronic properties of graphenylene behave considering different types, location and concentration of hydrogen/halogen atoms in the structure.

Bibliography

- [1] S. Dutta and S. K. Pati. Novel properties of graphene nanoribbons: a review. *Journal of Materials Chemistry*, 20(38):8207–8223, 2010.
- [2] R. Saito, G. Dresselhaus, and M. S. Dresselhaus. *Physical properties of carbon nanotubes*. World Scientific, 1998.
- [3] S. Iijima. Helical microtubules of graphitic carbon. *Nature*, 354(6348):56, 1991.
- [4] M. J. Madou. *From MEMS to Bio-MEMS and Bio-NEMS: Manufacturing Techniques and Applications*. CRC Press, 2011.
- [5] H. W. Kroto, J. R. Heath, S. C. O’Brien, R. F. Curl, and R. E. Smalley. C60: buckminsterfullerene. *Nature*, 318:162–163, 1985.
- [6] A. J. G. Zarbin and M. M. Oliveira. Nanoestruturas de carbono (nanotubos, grafeno): Quo vadis. *Química Nova*, 36(10):1533–1539, 2013.
- [7] E. Osawa, H. W. Kroto, P. W. Fowler, and E. Wasserman. The evolution of the football structure for the c60 molecule: A retrospective. *Philosophical Transactions: Physical Sciences and Engineering*, 1993.
- [8] H. W. Kroto. C60b buckminsterfullerene, other fullerenes and the icospiral shell. *Computers & Mathematics with Applications*, 17(1-3):417–423, 1989.
- [9] K. S. Novoselov, A. K. Geim, S. V. Morozov, D. A. Jiang, Y. Zhang, S. V. Dubonos, I. V. Grigorieva, and A. A. Firsov. Electric field effect in atomically thin carbon films. *Science*, 306(5696):666–669, 2004.
- [10] K. S. Novoselov, V. I. Fal, L. Colombo, P. R. Gellert, M. G. Schwab, K. Kim, et al. A roadmap for graphene. *Nature*, 490(7419):192, 2012.

- [11] A. S. Mayorov, R. V. Gorbachev, S. V. Morozov, L. Britnell, R. Jalil, L. A. Ponomarenko, P. Blake, K. S. Novoselov, K. Watanabe, T. Taniguchi, et al. Micrometer-scale ballistic transport in encapsulated graphene at room temperature. *Nano Letters*, 11(6):2396–2399, 2011.
- [12] S. Bae, H. Kim, Y. Lee, X. Xu, J-S. Park, Y. Zheng, J. Balakrishnan, T. Lei, H. R. Kim, Y. I. Song, et al. Roll-to-roll production of 30-inch graphene films for transparent electrodes. *Nature Nanotechnology*, 5(8):574, 2010.
- [13] J. S. Bunch, S. S. Verbridge, J. S. Alden, A. M. Van Der Zande, J. M. Parpia, H. G. Craighead, and P. L. McEuen. Impermeable atomic membranes from graphene sheets. *Nano Letters*, 8(8):2458–2462, 2008.
- [14] A. A. Balandin, S. Ghosh, W. Bao, I. Calizo, D. Teweldebrhan, F. Miao, and C. N. Lau. Superior thermal conductivity of single-layer graphene. *Nano Letters*, 8(3):902–907, 2008.
- [15] O. V. Yazyev. Emergence of magnetism in graphene materials and nanostructures. *Reports on Progress in Physics*, 73(5):056501, 2010.
- [16] R. M. Martin. *Electronic structure: basic theory and practical methods*. Cambridge university press, 2004.
- [17] J. Simons. *An introduction to theoretical chemistry*. Cambridge University Press, 2003.
- [18] A. H. C. Neto, F. Guinea, N. M. R. Peres, K. S. Novoselov, and A. Geim. The electronic properties of graphene. *Reviews of Modern Physics*, 81(1):109, 2009.
- [19] M. I. Katsnelson. Graphene: carbon in two dimensions. *Materials Today*, 10(1-2):20–27, 2007.
- [20] K. I. Bolotin, K. J. Sikes, Z. D. Jiang, M. Klima, G. Fudenberg, J. Hone, P. H Kim, and H. L. Stormer. Ultrahigh electron mobility in suspended graphene. *Solid State Communications*, 146(9-10):351–355, 2008.
- [21] F. Banhart, J. Kotakoski, and A. V. Krashennnikov. Structural defects in graphene. *ACS Nano*, 5(1):26–41, 2010.
- [22] H. Liu, Y. Liu, and D. Zhu. Chemical doping of graphene. *Journal of Materials Chemistry*, 21(10):3335–3345, 2011.

- [23] G. Z. Magda, X. Jin, I. Hagymási, P. Vancsó, Z. Osváth, P. Nemes-Incze, C. Hwang, L. P. Biro, and L. Tapasztó. Room-temperature magnetic order on zigzag edges of narrow graphene nanoribbons. *Nature*, 514(7524):608, 2014.
- [24] Q. Song, B. Wang, K. Deng, X. Feng, M. Wagner, J. D. Gale, K. Müllen, and L. Zhi. Graphenylene, a unique two-dimensional carbon network with nondelocalized cyclohexatriene units. *Journal of Materials Chemistry C*, 1(1):38–41, 2013.
- [25] A. Reina, X. Jia, J. Ho, D. Nezich, H. Son, V. Bulovic, M. S. Dresselhaus, and J. Kong. Large area, few-layer graphene films on arbitrary substrates by chemical vapor deposition. *Nano Letters*, 9(1):30–35, 2008.
- [26] E. Rollings, G-H. Gweon, S. Y. Zhou, B. S. Mun, J. L. McChesney, B. S. Hussain, A. V. Fedorov, P. N. First, W. A. De Heer, and A. Lanzara. Synthesis and characterization of atomically thin graphite films on a silicon carbide substrate. *Journal of Physics and Chemistry of Solids*, 67(9-10):2172–2177, 2006.
- [27] C. S. Park, H. Yoon, and O. S. Kwon. Graphene-based nanoelectronic biosensors. *Journal of Industrial and Engineering Chemistry*, 38:13–22, 2016.
- [28] R. S. Edwards and K. S. Coleman. Graphene synthesis: relationship to applications. *Nanoscale*, 5(1):38–51, 2013.
- [29] P. Yu, S. E. Lowe, G. P. Simon, and Y. L. Zhong. Electrochemical exfoliation of graphite and production of functional graphene. *Current Opinion in Colloid and Interface Science*, 20(5-6):329–338, 2015.
- [30] J. Lu, J. Yang, J. Wang, A. Lim, S. Wang, and K. P. Loh. One-pot synthesis of fluorescent carbon nanoribbons, nanoparticles, and graphene by the exfoliation of graphite in ionic liquids. *ACS Nano*, 3(8):2367–2375, 2009.
- [31] J. M. Tour. Top-down versus bottom-up fabrication of graphene-based electronics. *Chemistry of Materials*, 26(1):163–171, 2013.
- [32] K. S. Kim, Y. Zhao, H. Jang, S. Y. Lee, J. M. Kim, K. S. Kim, J. Ahn, P. Kim, J. Choi, and B. H. Hong. Large-scale pattern growth of graphene films for stretchable transparent electrodes. *Nature*, 457(7230):706, 2009.
- [33] T. Han, Y. Lee, M. Choi, S. Woo, S. Bae, B. H. Hong, J. Ahn, and T. Lee. Extremely efficient flexible organic light-emitting diodes with modified graphene anode. *Nature Photonics*, 6(2):105, 2012.

- [34] K. Kim, S. Bae, C. T. Toh, H. Kim, J. H. Cho, D. Whang, T. Lee, B. Ozyilmaz, and J. Ahn. Ultrathin organic solar cells with graphene doped by ferroelectric polarization. *ACS Applied Materials and Interfaces*, 6(5):3299–3304, 2014.
- [35] J. H. Ahn, B. H. Hong, F. Torrasi, J. N. Coleman, J. Liu, S. Böhm, M. Drndić, K. Kostarelos, K. Novoselov, and E. J. Siochi. Things you could do with graphene. *Nature Nanotechnology*, 9:737–47, 2014.
- [36] Y. Zhu, S. Murali, M. D. Stoller, K. J. Ganesh, W. Cai, P. J. Ferreira, A. Pirkle, R. M. Wallace, K. A. Cychoz, M. Thommes, et al. Carbon-based supercapacitors produced by activation of graphene. *Science*, 332(6037):1537–1541, 2011.
- [37] K. Kim, J. Choi, T. Kim, S. Cho, and H. Chung. A role for graphene in silicon-based semiconductor devices. *Nature*, 479(7373):338, 2011.
- [38] E. W. Hill, A. Vijayaraghavan, and K. Novoselov. Graphene sensors. *IEEE Sensors Journal*, 11(12):3161–3170, 2011.
- [39] L. Yang, L. Zhang, and T. J. Webster. Carbon nanostructures for orthopedic medical applications. *Nanomedicine*, 6(7):1231–1244, 2011.
- [40] N. Merino-Díez, J. Li, A. Garcia-Lekue, G. Vasseur, M. Vilas-Varela, E. Carbonell-Sanromà, M. Corso, J. E. Ortega, D. Peña, J. I. Pascual, et al. Unraveling the electronic structure of narrow atomically precise chiral graphene nanoribbons. *The Journal of Physical Chemistry Letters*, 9(1):25–30, 2017.
- [41] L. Pisani, J. A. Chan, B. Montanari, and N. M. Harrison. Electronic structure and magnetic properties of graphitic ribbons. *Physical Review B*, 75(6):064418, 2007.
- [42] Y-W. Son, M. L. Cohen, and S. G. Louie. Energy gaps in graphene nanoribbons. *Physical Review Letters*, 97(21):216803, 2006.
- [43] O. Rahaman, B. Mortazavi, A. Dianat, G. Cuniberti, and T. Rabczuk. A structural insight into mechanical strength of graphene-like carbon and carbon nitride networks. *Nanotechnology*, 28(5):055707, 2016.
- [44] E. Perim, R. Paupitz, P. Autreto, and D. S. Galvao. Inorganic graphenylene: a porous two-dimensional material with tunable band gap. *The Journal of Physical Chemistry C*, 118(41):23670–23674, 2014.

- [45] Z. Wang, X. Zhou, X. Zhang, Q. Zhu, H. Dong, M. Zhao, and A. R. Oganov. Phagraphene: a low-energy graphene allotrope composed of 5–6–7 carbon rings with distorted dirac cones. *Nano Letters*, 15(9):6182–6186, 2015.
- [46] B. Mortazavi, Z. Fan, L. F. C. Pereira, A. Harju, and T. Rabczuk. Amorphized graphene: A stiff material with low thermal conductivity. *Carbon*, 103:318–326, 2016.
- [47] J. L. Bredas and R. H. Baughman. Theoretical study of the electronic properties of biphenylene polymers: Prediction of new highly conducting polymer complexes. *Journal of Polymer Science: Polymer Letters Edition*, 21(6):475–479, 1983.
- [48] V. H. Crespi, L. X. Benedict, M. L. Cohen, and S. G. Louie. Prediction of a pure-carbon planar covalent metal. *Physical Review B*, 53(20):R13303, 1996.
- [49] H. Terrones, M. Terrones, E. Hernández, N. Grobert, J. C. Charlier, and P. M. Ajayan. New metallic allotropes of planar and tubular carbon. *Physical Review Letters*, 84(8):1716, 2000.
- [50] A. T. Koch, A. H. Khoshaman, H. D. E. Fan, G. A. Sawatzky, and A. Nojeh. Graphenylene nanotubes. *The Journal of Physical Chemistry Letters*, 6(19):3982–3987, 2015.
- [51] A. T. Balaban and K. P. C. Vollhardt. Heliphenes and related structures. *The Open Organic Chemistry Journal*, 5(1), 2011.
- [52] J. Cai, P. Ruffieux, R. Jaafar, M. Bieri, T. Braun, S. Blankenburg, M. Muoth, A. P. Seitsonen, M. Saleh, X. Feng, et al. Atomically precise bottom-up fabrication of graphene nanoribbons. *Nature*, 466(7305):470, 2010.
- [53] F. I. L. Passos, J. G. da Silva Filho, A. Saraiva-Souza, A. G. Souza Filho, V. Meunier, and E. C. Girão. One-and two-dimensional carbon nanostructures based on unfolded buckyballs: An ab initio investigation of their electronic properties. *Physical Review B*, 95(19):195124, 2017.
- [54] M. Born and R. Oppenheimer. Zur quantentheorie der molekeln. *Annalen der Physik*, 389(20):457–484, 1927.
- [55] J. Kohanoff. *Electronic structure calculations for solids and molecules: theory and computational methods*. Cambridge University Press, 2006.
- [56] J. C Slater. The theory of complex spectra. *Physical Review*, 34(10):1293, 1929.

- [57] V. Fock. Näherungsmethode zur lösung des quantenmechanischen mehrkörperproblems. *Zeitschrift für Physik*, 61(1-2):126–148, 1930.
- [58] C. C. J. Roothaan. New developments in molecular orbital theory. *Reviews of Modern Physics*, 23(2):69, 1951.
- [59] P. Hohenberg and W. Kohn. Inhomogeneous electron gas. *Physical Review*, 136(3B):B864, 1964.
- [60] W. Koch and M. C. Holthausen. *A chemist's guide to density functional theory*. John Wiley & Sons, 2015.
- [61] W. Kohn and L. J. Sham. Self-consistent equations including exchange and correlation effects. *Physical Review*, 140(4A):A1133, 1965.
- [62] E. Nakamachi, Y. Uetsuji, H. Kuramae, K. Tsuchiya, and H. Hwang. Process crystallographic simulation for biocompatible piezoelectric material design and generation. *Archives of Computational Methods in Engineering*, 20(2):155–183, 2013.
- [63] J. P. Perdew, K. Burke, and M. Ernzerhof. Generalized gradient approximation made simple. *Physical Review Letters*, 77(18):3865, 1996.
- [64] M. A. L. Marques and S. Botti. O que é e para que serve a teoria dos funcionais da densidade. *Gazeta de Física*, 29(4):10–15, 2006.
- [65] F. Bruneval and M. Gatti. *First Principles Approaches to Spectroscopic Properties of Complex Materials*, volume 347. edited by C. Di Valentin, S. Botti, and M. Cococcioni (Springer, Berlin, Heidelberg), 2014.
- [66] J. P. Perdew, A. Ruzsinszky, G. I. Csonka, O. A. Vydrov, G. E. Scuseria, L. A. Constantin, X. Zhou, and K. Burke. Restoring the density-gradient expansion for exchange in solids and surfaces. *Physical Review Letters*, 100(13):136406, 2008.
- [67] Z. Wu and R. E. Cohen. More accurate generalized gradient approximation for solids. *Physical Review B*, 73(23):235116, 2006.
- [68] L. He, F. Liu, G. Hautier, M. J. T. Oliveira, M. A. L. Marques, F. D. Vila, J. J. Rehr, G-M. Rignanese, and A. Zhou. Accuracy of generalized gradient approximation functionals for density-functional perturbation theory calculations. *Physical Review B*, 89(6):064305, 2014.

-
- [69] J. M. Soler, E. Artacho, J. D. Gale, A. García, J. Junquera, P. Ordejón, and D. Sánchez-Portal. The siesta method for ab initio order-n materials simulation. *Journal of Physics: Condensed Matter*, 14(11):2745, 2002.
- [70] D. R. Hamann, M. Schlüter, and C. Chiang. Norm-conserving pseudopotentials. *Physical Review Letters*, 43(20):1494, 1979.
- [71] N. Troullier and J. L. Martins. Efficient pseudopotentials for plane-wave calculations. ii. operators for fast iterative diagonalization. *Physical Review B*, 43(11):8861, 1991.
- [72] L. Kleinman and D. M. Bylander. Efficacious form for model pseudopotentials. *Physical Review Letters*, 48(20):1425, 1982.
- [73] K. Nakada, M. Fujita, G. Dresselhaus, and M. S. Dresselhaus. Edge state in graphene ribbons: Nanometer size effect and edge shape dependence. *Physical Review B*, 54(24):17954, 1996.
- [74] J. Fernández-Rossier and J. J. Palacios. Magnetism in graphene nanoislands. *Physical Review Letters*, 99(17):177204, 2007.
- [75] W. L. Wang, O. V. Yazyev, S. Meng, and E. Kaxiras. Topological frustration in graphene nanoflakes: magnetic order and spin logic devices. *Physical Review Letters*, 102(15):157201, 2009.
- [76] J. K Bhattacharjee and B. K. Chakrabarti. Frontiers in condensed matter physics. *Indian Journal of Physics*, 5, 2005.
- [77] W Liu, J. Liu, and M. Miao. Band gap engineering of graphenylene by hydrogenation and halogenation: a density functional theory study. *RSC Advances*, (5), 2015.